AN ABSTRACT OF THE THESIS OF

Alexander J. Mieloszyk for the degree of Honors Baccalaureate of Science in Nuclear Engineering presented on May 26, 2010.
Title: Vacuum Testing of a Small Radioisotope Thermoelectric Generator

Abstract approved: _____
Brian Woods

Radioisotope Power Systems (RPS's) are a key element to NASA's deep space exploration programs. As NASA looks towards new generations of smaller, modular spacecraft, appropriately smaller RPS's will be needed. The Single General Purpose Heat Source Radioisotope Thermoelectric Generator (S-GPHS-RTG) has been developed to fill this role. The S-GPHS-RTG will utilize one GPHS to provide 250 W_t which will be ideally be converted to 20-25 W_e by Thermoelectric Converters (TEC's). Using a full scale model S-GPHS-RTG in a vacuum chamber, 250 W_t was applied via an electrically powered model GPHS, and steady-state temperatures were observed. As part of these tests, multiple insulation packages were investigated, including: Multi Layer Insulation (MLI), silica fiber, and various aerogel combinations. The vacuum conditions were intended to simulate space conditions the S-GPHS-RTG will experience as it travels through space. The steady-state temperatures it experiences will largely affect its performance as a power source, as the TEC's ability to convert heat to electricity is dependent on the temperature gradient they experience. A virtual model of the experiment was also created in Thermal Desktop in an attempt to simulate it. However, this virtual model failed to generate accurate results.

Keywords: Radioisotope Thermoelectric Generator, RTG, General Purpose Heat Source, GPHS, Multi Layer Insulation, MLI, aerogel, Thermal Desktop

Corresponding e-mail address: amieloszyk@gmail.com

Vacuum Testing of a Small Radioisotope Thermoelectric Generator

By

Alexander J. Mieloszyk

A PROJECT

Submitted to

Oregon State University

University Honors College

in partial fulfillment of
the requirements for the
degree of

Honors Baccalaureate of Science in Nuclear Engineering

Presented May 26, 2010
Commencement June 2010

Honors Baccalaureate in Nuclear Engineering project of Alexander J. Mieloszyk

presented on May 26, 2010.

APPROVED:

Mentor, representing Nuclear Engineering and Radiation Health Physics

---

Committee Member, representing Oregon NASA Space Grant Consortium

---

Committee Member, representing NASA Ames Research Center

Chair, Department of Nuclear Engineering and Radiation Health Physics

---

Dean, University of Honors College

I understand that my project will become part of the permanent collection of Oregon State University, University Honors College. My signature below authorizes release of my project to any reader upon request.

Alexander J. Mieloszyk, Author

ACKNOWLEDGEMENTS

I would like to thank Ali Kashani and Ben Halvenjstein for their patience and guidance in helping to make this project a reality, as well as sacrificing their lab space to my work. I would also like to acknowledge Brian Woods for directing me to this project and being a constant resource for me when I needed direction. The Oregon NASA Space Grant Consortium played a huge role by funding all of my work on this project. Without my mother, Karyn Mieloszyk, and Carissa Pocock's help editing, this thesis would not be anywhere near as polished as it currently is. This thesis is also a reflection of every friendship that I have been lucky enough to foster in my four years at Oregon State University, without them I never could have made it to this point. Lastly, I'd like to thank my parents, Jim and Karyn Mieloszyk, for teaching me to never settle for anything less than my best effort and constantly motivating me to grow into something better.

TABLE OF CONTENTS

1. **DEFINITIONS……...……1**
2. **INTRODUCTION……..……2**
3. **LITERATURE REVIEW……..…7**
4. **MATERIALS AND METHODS……12**
5. **TEST RESULTS……...……38**
6. **DISCUSSION……...……54**
7. **CONCLUSIONS……...…59**
8. **BIBLIOGRAPHY……62**

LIST OF FIGURES

Figure **Page**

Figure 1. Diagram of the GPHS-RTG…….....4

Figure 2. Top view of S-GPHS-RTG……...….12

Figure 3. Photo of model GPHS…….....14

Figure 4. Exploded view of S-GPHS-RTG-1 …….....15

Figure 5. Photograph of aluminum spacers…….....….17

Figure 6. Exploded view of S-GPHS-RTG-2…….....…..19

Figure 7. Example of S-GPHS-RTG-2 modular stacking…….…….....20

Figure 8. S-GPHS-RTG-2 experimental setup…….....21

Figure 9. Thermocouple locations on the S-GPHS-RTG-1……..……...…...27

Figure 9. Thermocouple locations on the S-GPHS-RTG-1……..…….....28

Figure 11. Thermocouple locations on the S-GPHS-RTG-2……...…….....28

Figure 12. Thermocouple locations on the S-GPHS-RTG-2…….....…..29

Figure 13. Aerogel thermal conductivity values used in Thermal Desktop calculations.…….....32

Figure 14. Thermal Desktop results for external components of 2006 OSU testing…….36

Figure 15. Thermal Desktop results for internal components of 2006 OSU testing…….36

Figure 16. Photograph of damaged MLI from S-GPHS-RTG-1 Test #1…….....….39

Figure 17. Transient temperatures of S-GPHS-RTG-1 external components using MLI/silica fiber……...….41

Figure 18. Transient temperatures of S-GPHS-RTG-1 external components using MLI/silica fiber……...….42

Figure 19. Transient temperatures of S-GPHS-RTG-2 TEC graphite……..……..…….49

Figure 20. Transient temperatures of S-GPHS-RTG-2 shell……...….49

Figure 21. Thermal Desktop prediction of S-GPHS-RTG-1 steady state temperatures……...51

Figure 22. Thermal Desktop prediction of S-GPHS-RTG-2 internal steady state temperatures……...52

Figure 23. Thermal Desktop prediction of S-GPHS-RTG-2 external steady state temperatures……..……53

Figure 24. GPHS maximum temperature comparison……...……..….55

Figure 25. Comparison of TEC temperature gradients ……..……..….56

Figure 26. Comparison of fin temperature gradients …….....…….58

LIST OF TABLES

Table **Page**

Table 1. S-GPHS-RTG-1 Test Matrix……..…….23

Table 2. S-GPHS-RTG-2 Test Matrix……..…….25

Table 3. Thermocouple locations……....….27

Table 4. Material Properties used in Thermal Desktop calculations……..……..….33

Table 5. Steady state temperatures of ambient atmosphere S-GPHS-RTG-1 tests……...….35

Table 6. Maximum temperatures of S-GPHS-RTG-1 test using MLI…….....….39

Table 7. Steady state temperatures of S-GPHS-RTG-1 tests using MLI/silica fiber……....40

Table 8. Steady state temperatures of S-GPHS-RTG-2 tests using Cabot/ Thermablok aerogel……44

Table 9. Steady state temperatures of uninsulated S-GPHS-RTG-2……...…….45

Table 10. Steady state temperatures of S-GPHS-RTG-2 tests using Cabot aerogel……....47

Table 11. Steady state temperatures of S-GPHS-RTG-2 test using Thermablok aerogel……...….48

Table 12. Thermal Desktop prediction of S-GPHS-RTG-1 steady state temperatures ……..50

Table 13. Thermal Desktop prediction of S-GPHS-RTG-2 steady state temperatures……...52

LIST OF EQUATIONS

Equation **Page**

(1)……..……...…….45

(2)……..……...….45

(3)……..……...…….45

(4)……..……...…….45

Vacuum Testing of a Small Radioisotope Thermoelectric Generator

1. DEFINITIONS

ARC	NASA Ames Research Center
DOE	Department of Energy
GPHS	General Purpose Heat Source
JPL	Jet Propulsion Laboratory
LWRHU	Light Weight Radioisotope Heater Unit
MLI	Multi Layer Insulation
MMRTG	Multi Mission RTG
MSL	Mars Science Laboratory
NASA	National Aeronautics and Space Administration
OSU	Oregon State University
RPS	Radioisotope Power System
RTG	Radioisotope Thermoelectric Generator
S-GPHS-RTG	Single GPHS RTG
S-GPHS-RTG-1	First Generation S-GPHS-RTG (2006-2008)
S-GPHS-RTG-2	Second Generation S-GPHS-RTG (2009-current)
SRG	Stirling Radioisotope Generator
TC	Thermocouple
TEC	Thermoelectric Converter
VIP	Vacuum Insulation Panel
W_e	Watts Electric
W_t	Watts Thermal

2. INTRODUCTION

Since 1961, NASA has utilized RPS's in both manned and unmanned space missions.[1] Of particular importance is the RTG, which has a proven track record for missions to the inner and outer solar system and beyond. Unlike SRG's, RTG's have no moving parts and utilize flight-tested and reliable technology. Because the decay of Plutonium 238 within RTG's provides a constant heat source, they are not vulnerable to many of the disadvantages of solar power. Power is supplied 24 hours a day, regardless of lighting conditions. RTG's also remain unaffected by damage from particulates, like dust or sand, to its surfaces. These attributes make RTG's particularly appealing for surface missions to Mars where high latitude operation or winter survival is needed. Independence from solar flux also makes RTG's extremely valuable for deep space missions.

The heat source for large (multi-Watt) RPS systems is the GPHS. Currently NASA utilizes the Step 2 GPHS, which is a more robust version of the heritage GPHS. Within the GPHS are four iridium-clad PuO_2 fuel pellets which provide 250 W_t from the decay heat of the Pu-238. These pellets are encased in layers of various carbon-based aeroshells which are intended to provide protection from break up in the event the GPHS experiencing an atmospheric reentry.[2] In total, each GPHS contains approximately 600 grams of PuO2. [3] GPHS's are rectangular in shape and are intended to be stacked together to provide thermal power as high as 4300 W_t. [4] The GPHS is a highly versatile heat source, having been used in many RTG and SRG designs while undergoing relatively few design changes itself.

Power conversion in RPS's is obviously a very important component of the design. SRG's utilize a Stirling converter to mechanically convert the heat into electricity.

RTG's, on the other hand, employ TEC's which directly convert the heat into electricity as it passes through. TEC's, unlike Stirling converters, have no moving parts, making them a more mechanically resilient power conversion option. TEC's operate on the basis of the Seebeck effect, which occurs when a conductor or semiconductor experiences a temperature gradient, giving rise to an electric field. This voltage can be measured at the junction of two dissimilar metals. [4] It is this same effect that allows thermocouples to measure temperature. In current RTG's, a silicon-germanium TEC is used to achieve approximately 8% conversion rates. Future developments show promise of raising the efficiency of TEC's to 14-16%.[3] Because the temperature gradient drives the TEC's ability to convert heat to electricity, maximizing this gradient is extremely critical.

Because RPG's are designed to work in space conditions, heat rejection is almost an entirely radiative process. Cooling fins are used on the exterior of the devices to increase the surface area over which heat may be dissipated.

NASA currently employs the GPHS-RTG, as seen in Figure 1, and Multi-Mission RTG (MMRTG) which provide 285 W_e and 110 W_e respectively.[3] RTG's have powered mankind's farthest exploration of our solar system and missions that are well on their way to interstellar space. These missions include Pioneer 10 and 11, Cassini, Galileo, Ulysses, New Horizons, Viking 1 and 2, and Voyager 1 and 2. Currently, the MMRTG is scheduled to be used on the next Mars surface mission, the MSL. That mission will place the largest and most capable rover to date on Mars. That rover will be able to range farther than previous generations, operating day and night without restriction from the sun. Largely thanks to the MMRTG, the MSL will also be able to survive harsh Martian

winters by utilizing waste supplied by the MMRTG. RTG technology quite simply makes these missions possible, thanks to its reliability, durability, and independence. [5]

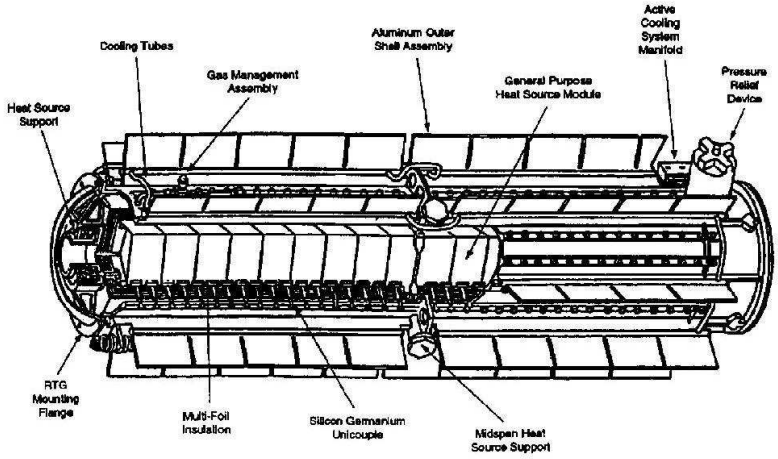

Figure 1. Diagram of the GPHS-RTG[1]

The S-GPHS-RTG is a proposed RPS designed to provide the benefits of large RTG's to smaller missions that require significantly less power than current RTG power sources provide. The S-GPHS-RTG has also been designed so that more than one unit can be fastened together to provide additional power. This modular capability allows the S-GPHS-RTG to fulfill the requirements of a wider range of missions that do not require the larger power systems. This will open the doors for a new generation of small spacecraft to explore areas where they previously have been constrained by a lack of solar energy.

The S-GPHS-RTG was originally designed and analyzed by JPL. A full scale model was then built and tested in ambient atmosphere at OSU in 2006. This test was intended to determine what temperatures would be seen during Earth storage of the S-GPHS-RTG.[6] Due to the fact that these tests used a ceramic furnace insulation that was not

likely to be used in future versions of the device and did not include any testing under vacuum conditions, further testing was called for. The model S-GPHS-RTG used at OSU in 2006 was available for use, and thus the same device was reused in 2008 for tests at ARC.

Because of the importance of maintaining a large temperature gradient across the TEC's, the performance of the S-GPHS-RTG's insulation will play a major role in the device's ability to provide electrical power. The purpose of this study is to investigate the feasibility of various insulation packages in a full size model S-GPHS-RTG under vacuum conditions. This is intended to simulate conditions that the S-GPHS-RTG will experience during space travel. Insulation packages that were considered for this study included traditional MLI's and varying forms of aerogel insulation.

MLI is an extremely effective insulator under vacuum conditions where radiative heat transfer becomes a more dominant heat loss mechanism. The tests performed at ARC in 2008 made use of this insulation. The tests yielded varied results, giving rise to the suggestion that aerogel materials may be a better solution. Based off these suggestions, the 2009 test series used aerogel insulations.

Aerogel is a material whose structure is mostly empty space. Under atmospheric conditions, this space is filled by air. Because of this, aerogel is extremely lightweight and has a thermal conductivity that approaches that of air. One of aerogel's most appealing attributes is that it can take many forms, including small granules that may simply be poured into the space to be insulated.

Vacuum testing of RTG's can be a very time intensive process. Because of this, the potential ability to optimize a design and insulation package within a computer model

becomes extremely valuable. Thermal Desktop is a thermal analysis software that allows models to be built and tested in AutoCAD Mechanical. A significant part of this study, for both the 2008 and 2009 tests, was based around attempting to build an accurate model that would allow more rapid virtual testing to occur.

3. LITERATURE REVIEW

Woods, et al. tested the first generation S-GPHS-RTG under atmospheric conditions at OSU. These tests were aimed primarily to provide physical data for the validation of numerical thermal analyses of the S-GPHS-RTG. A model S-GPHS-RTG was built from aluminum for the study. For the insulation package, a ceramic insulating board was used. The GPHS was simulated with a graphite block and resistance wires. Type K thermocouples were used to record temperatures throughout the S-GPHS-RTG at a full steady state power of 250 W_t.[6]

While these tests were not under vacuum conditions and utilized a very different insulation package, many of the test processes were utilized in this study. The same S-GPHS-RTG shell used at OSU was also used in the 2008 tests at ARC. Also, the majority of thermocouple locations were replicated in this study. This provided for a direct comparison of the effects of different insulations and vacuum conditions. TEC's were modeled similarly as graphite plates attached to the shell via tungsten rods. The maximum GPHS temperatures observed in the 2006 OSU tests were approximately 410˚C. The model TEC's observed temperature gradients of approximately 180˚C. It is worth noting that the maximum observed GPHS temperature failed to meet the design temperature of 1100˚C.[6]

Balint and Emis developed a numerical model in an attempt to simulate the test conditions of the OSU testing by Woods, et al. The purpose of the development of this virtual model is to validate the code for future work with the S-GPHS-RTG. The model incorporated the graphite heater which modeled the GPHS, the graphite shoes of the modeled TEC's, ceramic insulation, and aluminum shell of the S-GPHS-RTG.

Convection was enabled between the graphite block, TEC shoes, and internally exposed insulation, as well as between the external components and the open atmosphere. Thermal connections were made between all components in direct contact, as well as the TEC shoes and external shell to model the tungsten component of the TEC's. The virtual model showed good agreement with the OSU tests for the external components, however, the internal components were incorrect by margins of over 100˚C. The cause of this difference was explained by geometric and material inconsistencies between the model and the physical test. The thermal resistance of the top plate being bolted on and not welded into place was a cause for concern, as it impedes heat dissipation to the cooling fins. This study also concluded that the cooling fins utilized by the S-GPHS-RTG design were indeed effective for heat removal under atmospheric conditions. [7]

Fricke et al. investigated the performance of VIP's over time. Of particular concern for their research was how increasing pressure within the panels would affect their insulating properties. Because these panels are flat, some sort of internal support must be incorporated. As part of this study, silica aerogels were used as fillers within the panels. The thermal conductivity was plotted over various pressures between 1 mbar and 1000 mbar. These curves suggested that between 10 mbar and 1000 mbar the conductivity of the silica aerogel decreased from about 25 mW/m/K to approximately 9 mW/m/K. This large decrease is the result of removing the air from the empty space of the aerogel. Without that air present to transfer heat, the heat must be conducted entirely through the silica frame, which due in part to its relatively small structure increases thermal resistance. [8]

Schmidt and Houts studied how nuclear power systems have been utilized in the past and the role that they will play in NASA's future space exploration plans. With the exception of one fission system, SNAP-10A, the US has only fielded radioisotope decay systems. Currently the MMRTG and SRG are being developed to supplement the GPHS-RTG, producing 120 W_e. While the Stirling converter of the SRG provides a higher specific power than the TEC's of the MMRTG, it has not yet been flight-tested and is still being developed. The MMRTG on the other hand is slated to provide power to the MSL on the surface of Mars. The next phase of development would call for the creation of high-power radioisotope systems. These systems would utilize either Stirling converters or next generation TEC's to provide power levels up to 1-2 kW_e. These power sources could be used for highly capable rovers, crew vehicles, habitation, etc. For longer duration surface habitation, an even larger power source is going to be required. Due to a need for higher specific power, this will likely require a reactor over radioisotope systems. These systems will likely provide 10-40 kW_e and utilize the same power conversion techniques employed by RPS's. The implementation of this strategy is expected to be gradual over the course of the next 30 or more years. The plan's success is also highly dependent on the development of advanced energy conversion systems and the DOE's ability to provide the necessary fuel. [9]

Rinehart provides an overview of RPS design characteristics. The study focuses mainly on fuel characteristics and heat source construction. An overview of past RPS usage in NASA missions is also included. A detailed radiological analysis of the PuO_2 fuel used within RPS's is performed. The methods used by the DOE for Pu purification for space fuels are shown. The paper also explicitly explains the construction methods

used for RPS heat sources. There is also an overview of GPHS-RTG's given, including their use of 18 GPHS's, 572 silicon/germanium TEC's, and 4300 W_t, as well as their ability to provide 285 W_e at 28 V. GPHS and LWRHU construction and components are explained, including their use of fuel cladding and aeroshells to protect the fuel from possible atmospheric reentry. Lastly, Rinehart gives estimates for how much Pu-238 is going to be needed to meet NASA's need to operate future missions using RPS's. [1]

Pantano and Hill performed thermal analyses of the newer Step 2 GPHS. The Step 2 GPHS is a more robust and larger version of the same heat source flown on previous missions, and was used on Cassini, Galileo, and Ulysses. The paper provides detailed information on design changes that have been made to the Step 2 GPHS, including replacing internal voids with aeroshell material and the addition of a gap between fuel pellets. The purpose of the paper is to establish a 3-D model of the Step 2 GPHS in Thermal Desktop. The study used two different boundary conditions, including simple radiation and operational conditions representative of the 110 W_e SRG. A 2.6 disk was modeled as the heat collector and was set to remain at 680˚C, which is the operating temperature of the hot face during normal operation. It was also assumed that all dimensions within the model are static, despite thermal expansion and other external forces. Different contact conductance was used for varying methods of thermal engagement, however, when in question conductance was over-estimated to provide a more conservative estimate. To simulate a Martian atmosphere, a 100% CO2 cover gas was used, as well as 100% Argon or Xenon environments for Earth storage. To model the radiation, a Monte Carlo ray-tracing algorithm was used with an upper limit of 20,000 rays per node. The simulation was run and iteratively adjusted until the benchmark of

1074˚ C at the aeroshell was achieved. This acted as a means of calibration. The calibrated model was then tested using various conditions, with and without the heat collector, different cover gases, etc. The testing proved to be consistent with previously collected data on heritage GPHS modules. It is thought that this Step 2 GPHS thermal model is appropriately accurate for use in a model of the 110 W_e SRG. [2]

4. MATERIALS AND METHODS

The S-GPHS-RTG utilizes a single GPHS as a heat source. That GPHS is located within an aluminum shell and surrounded radially by eight TEC's. The TEC's extend from the interior edge of the cylindrical portion of the S-GPHS-RTG's shell. This creates an octagon within the cylindrical portion of the shell. In the center of this octagon sits the GPHS. The GPHS's corners are oriented equidistantly with four corners of the TEC octagon, as seen in Figure 2. There is nothing but void space between the adjacent GPHS and TEC faces. The heat is transferred from the GPHS to the TEC's by thermal radiation, which becomes much more dominant at high temperatures and vacuum conditions. This space also protects the TEC's from the vibrations of the heavy GPHS during launch.

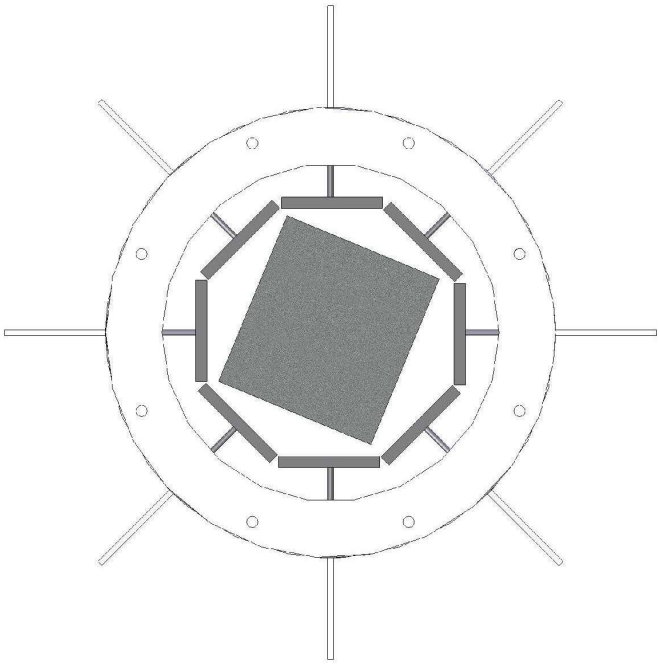

Figure 2. Top view of S-GPHS-RTG

For these tests, the TEC's were simulated by graphite plates attached to tungsten rods, which were affixed to the interior of the aluminum shell.

The 2008 and 2009 tests utilized two different shell designs for the S-GPHS-RTG. This was the result of a redesign prior to the 2009 testing which was intended to improve thermal symmetry. In order to differentiate between these two designs, the 2008 and 2009 S-GPHS-RTG's will be referred to as S-GPHS-RTG-1 and S-GPHS-RTG-2, respectively. Any references to S-GPHS-RTG will indicate shared design features.

The GPHS uses four iridium clad PuO_2 fuel pellets that provide 250 W_t of decay heat. These fuel pellets are embedded in a graphite aeroshell. For these tests, real plutonium was not used. Rather, the plutonium's decay heat was simulated by electric resistance heaters within a model GPHS. Marshall Space Flight Center supplied the heater, which is intended to specifically model the GPHS. This model GPHS is 3.66 inches x 4 inches x 2.25 inches and is a nearly exact replica of a GPHS. There also two electrical leads, which stand vertically from the top face of the heater. Holes diameter 0.25 inches, were drilled in the lid of the S-GPHS-RTG to allow access to these leads. The resistance of the heater element between the leads was measured to be 4.5 ohms. It was also discovered that a short circuit existed somewhere within the model GPHS which allowed electrical conduction via its outer surface. Because of this, extra care was taken to electrically isolate the model GPHS. Within the device, the GPHS was placed on insulating material to prevent conduction. The S-GPHS-RTG was supported by a titanium wire cradle, discussed in detail later. Insulting pads were placed below the support structures to prevent the GPHS's short circuit from conducting to the vacuum chamber, becoming a safety issue. Figure 3, below, is a photograph of the model GPHS used in these tests, with a quarter and ruler to illustrate its size.

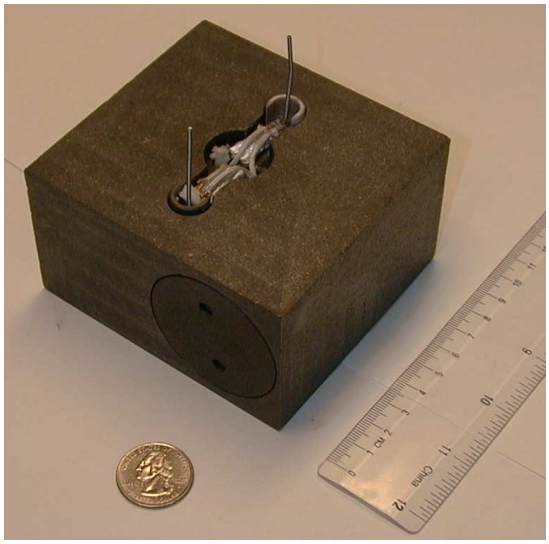

Figure 3. Photo of model GPHS

The shell of the S-GPHS-RTG-1 is a cylinder that has an internal diameter of 6.75 inches, a height of 1.7 inches, and a thickness of 0.125 inches. On the bottom of the cylinder, a disk with a diameter of 6.75 inches and a thickness 0.125 inches has been welded into place. On the top of the cylinder, a 0.9 inch wide ring with an inner diameter of 6.75 inches and a thickness of 0.32 inches has been welded into place to act as a lip. Eight fins, 2.15 inches tall, 3.25 inches long, and 0.15 inches thick have been welded vertically to both the cylinder and the bottom plate. A top plate with a diameter of 8.55 inches and a thickness of 0.32 inches is bolted to the lip at eight points. All external components of the S-GPHS-RTG-1 are made from alloy 6061 aluminum.

On the inside of the S-GPHS-RTG-1 shell are eight tungsten rods, diameter 0.125 inches and length 0.5 inches, aligned with each fin. These tungsten rods represent the TEC's and the cold side of the thermoelectric junction. The hot end of the thermoelectric junction is represented by eight graphite plates, which are attached to the tungsten rods. These plates are 2 inches square, and 0.25 inches thick.

These eight shoes are arranged to directly correspond to the eight aluminum fins. The tungsten rods are affixed at one end midway between top and bottom shell plates to the interior surface of the shell. The opposite end of the rod is then attached to a graphite shoe.

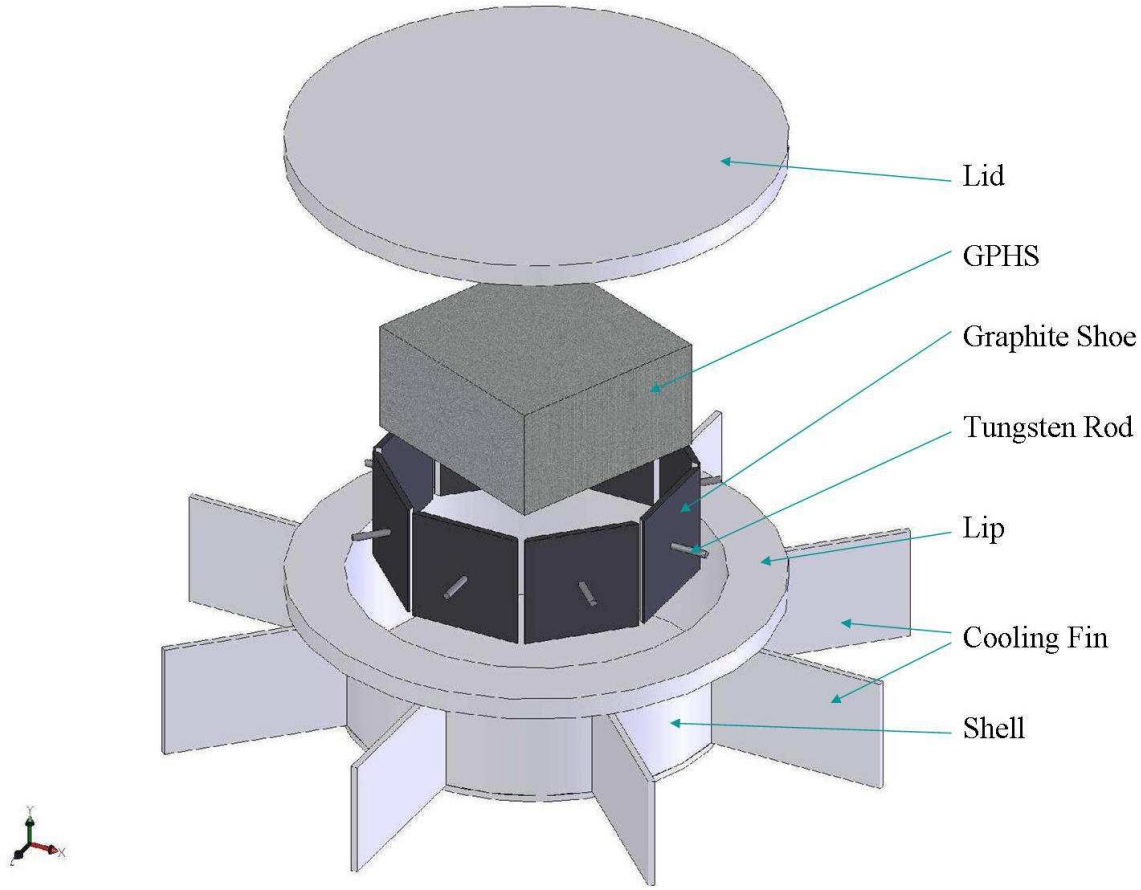

Figure 4. Exploded view of S-GPHS-RTG-1

Unfortunately, there was a major discrepancy in the design of the S-GPHS-RTG-1 and the model GPHS. The heater block originally used in the OSU test simply modeled the GPHS as a graphite block with an internal heater. This test utilized an electrically powered model GPHS. This presented a challenge, as the size of the graphite block used in the OSU experiment was slightly smaller than the model GPHS. The principle size

difference was in the height of the model GPHS. The original OSU design called for the GPHS to be 2 inches tall, opposed to the model GPHS's height of 2.25 inches.

There was not sufficient funding to build a new shell for the S-GPHS-RTG-1 that would sufficiently house the GPHS. To counteract the problem with the GPHS's height, aluminum spacers were placed between the lip and the lid. These spacers were cut from rectangular rods of alloy 6061 aluminum. They measure 2.4 inches long, 1 inch wide, and 0.4 inches tall.

Thermally, these spacers presented a problem for the already tenuous symmetry of the shell. In the OSU tests, the top plate became hotter than the bottom, because it lacked a thermal connection with the fins, and had poor thermal contact with the shell lip. Adding spacers was expected to intensify this problem if no corrective action was taken. To help insure good thermal contact, lead foil was placed between the lid, lip, and spacers.

This created a situation where the top plate of the shell was not in contact with the insulation covering the top of the model GPHS. However, the model GPHS was allowed to rest with its full weight on the insulation placed underneath it. This allowed superior thermal contact with the bottom insulation, and thus a less resistant path for the heat flow to the bottom of the aluminum shell.

Providing that equal thermal contact between the model GPHS and insulation was achieved on both the top and bottom surfaces, the design of the S-GPHS-RTG-1's shell was prone to thermal asymmetries. The top plate of the first generation aluminum shell was approximately a quarter inch thick, while the bottom plate was about half that thickness. The top plate was not permanently fixed to rest on the shell, rather being bolted on. This provided radically different thermal contact than the bottom plate, which

was firmly welded to the shell. A large lip was also welded to the top, but not bottom, of the first generation aluminum plate to allow the top plate to be attached. The use of aluminum spacers to provide room for the model GPHS likely only exacerbated this problem.

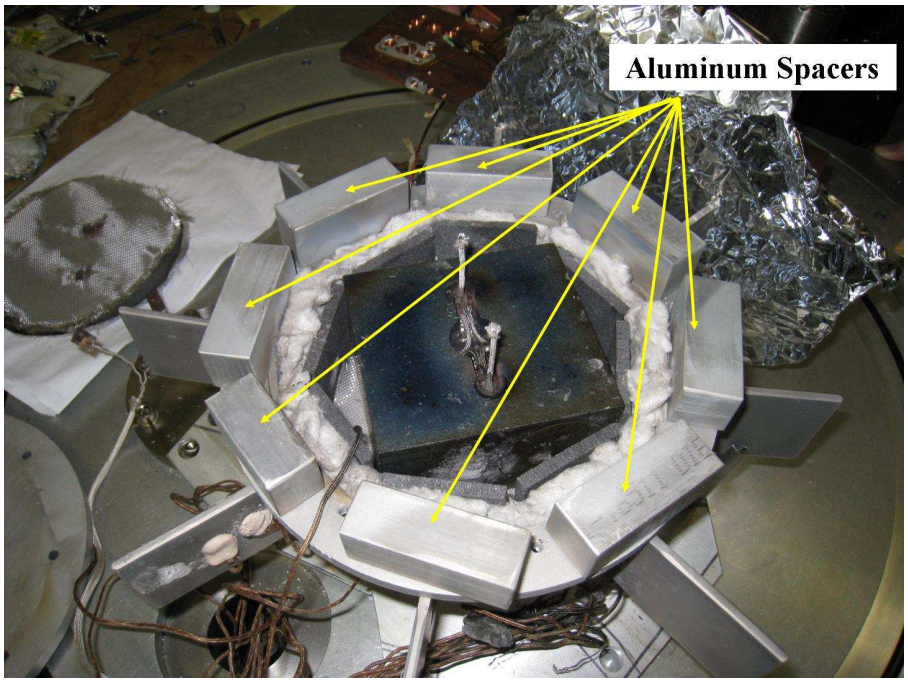

Figure 5. Photograph of aluminum spacers

These issues are the suspected cause of the differences seen in the steady state temperatures between the top and bottom of the S-GPHS-RTG during the 2008 ARC test. Because the root cause of these problems was the design of the first generation aluminum shell, a new shell was designed as the remedy.

The design of the S-GPHS-RTG-2's shell is aimed to correct three specific problems that existed previously. Two of those three issues, the vertical asymmetry and lack of necessary height, are detailed above. The third issue was that the interior of the S-GPHS-RTG-1 was barely large enough to accommodate all of the device's internal components.

To allow appropriate vertical space, the internal height of the S-GPHS-RTG-2 was increased from 2.55 inches to 3.25 inches. In order to insure vertical thermal symmetry, a lip was welded to both the top and bottom of the shell, and both the top and bottom plates were of equal thickness and used the same method of attachment via bolts. The radius of the cylinder was also increased to allow for more space between the S-GPHS-RTG's internal components. The S-GPHS-RTG-2 was redesigned using SolidWorks.

The internal diameter of the cylinder, which comprises the main body of the S-GPHS-RTG-2, is 7.5 inches, with a cylindrical wall thickness of 0.25 inches, giving an external diameter of 8 inches. The cylinder is 3 inches in height. At the top and bottom of the cylinder, a lip has been welded in place with an internal diameter of 7.5 inches, an external diameter of 10 inches, and a thickness of 0.125 inches. The eight fins are the same height as the cylinder, 3.25 inches in length, 0.125 inches thick, and are welded to the cylinder and both lips. The top and bottom of the S-GPHS-RTG-2 are sealed shut by discs 10 inches in diameter and 0.125 inches thick. Eight holes were drilled in the lips and discs which allowed them to be secured to one another with 0.25 inch bolts. A 0.5 inch diameter hole was also drilled near the bottom of the cylinder and covered on both sides by patches of silica woven blanket. These holes allowed gases to flow out of the S-GPHS-RTG-2 and ensure internal vacuum conditions and provided an entry point for the internal thermocouples. All aluminum used in the construction of the S-GPHS-RTG-2's shell is Aluminum 6061 T6. The GPHS's top and bottom faces are separated from the shell by approximately 0.4 inches of insulation.

The model TEC's are then arranged radially in line with each fin at the midpoint of the cylindrical component of the shell's height. The graphite plates are 2.25 inches in length

and width, and 0.25 inch thick high density isomolded graphite. The tungsten rods are 0.75 inch long, 0.325 inch diameter welding rods.

The increased size of the S-GPHS-RTG-2 also means that the surface area exposed to radiate heat to the environment has increased compared to the S-GPHS-RTG-1. Because both designs are ultimately dispersing the same amount of heat, we can expect the S-GPHS-RTG-2 to have lower external temperatures correlating to the increase in surface area.

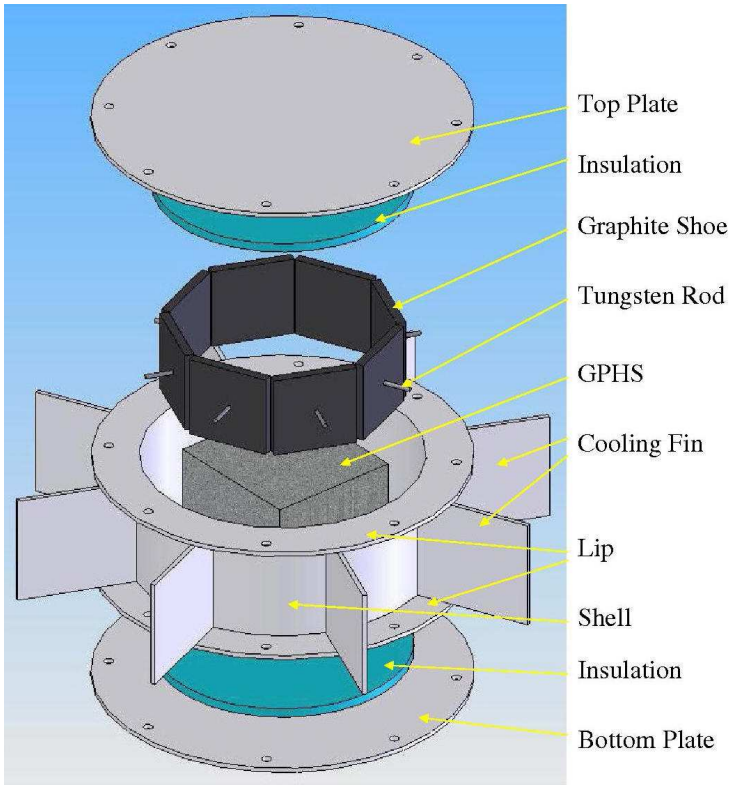

Figure 6. Exploded view of S-GPHS-RTG-2

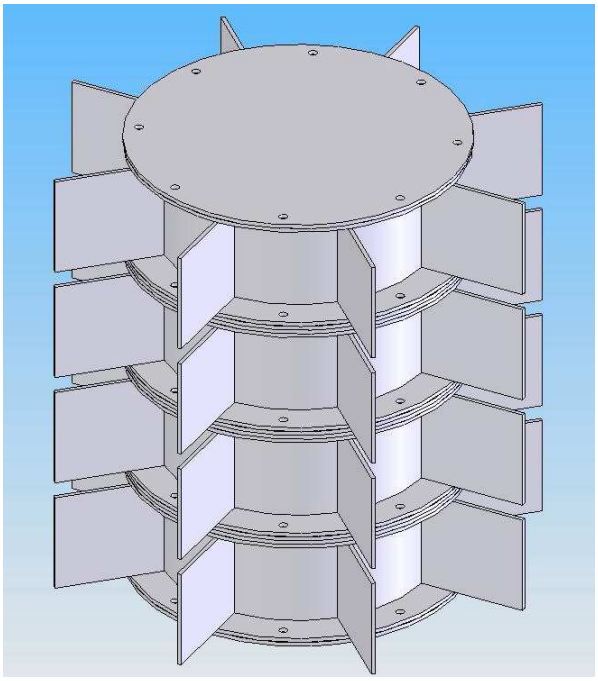

Figure 7. Example of S-GPHS-RTG-2 modular stacking

Within the vacuum chamber, the S-GPHS-RTG-1 was supported by four stainless steel tubes, which were constructed to attach to the fins. The tubes were approximately six inches long and half an inch in diameter. The tubes were supported at the bottom by an aluminum plate. Because the tubes had very thin walls and lacked a good thermal contact with the fins, the heat loss through them was considered negligible.

In order to prevent major heat loss through conduction, it was decided to suspend the S-GPHS-RTG over the base of the vacuum chamber. To do this, a base was constructed with aluminum plates which held four thin-walled aluminum tubes vertically. These tubes stood approximately one foot in height, with a hole drilled near the top. All four tubes were further secured to the base with titanium wire. Single strand titanium wire was then threaded through a fiberglass sheath. Two such wires were tied between the holes in aluminum tubes on opposing corners of the stand. The crossing wires provided a

convenient cradle in which the S-GPHS-RTG-2 was suspended. This stand is pictured in Figure 8. Minimal conductive heat transfer was allowed to occur between the S-GPHS-RTG and the vacuum chamber through the fiberglass sheathed wires. Because of a shorted circuit (~250 Ohms) in the model GPHS, which existed prior to the 2008 ARC tests, the S-GPHS-RTG's stands were placed on small pieces of insulation to completely prevent any shorts to the exterior of the vacuum chamber (not pictured in Figure 8).

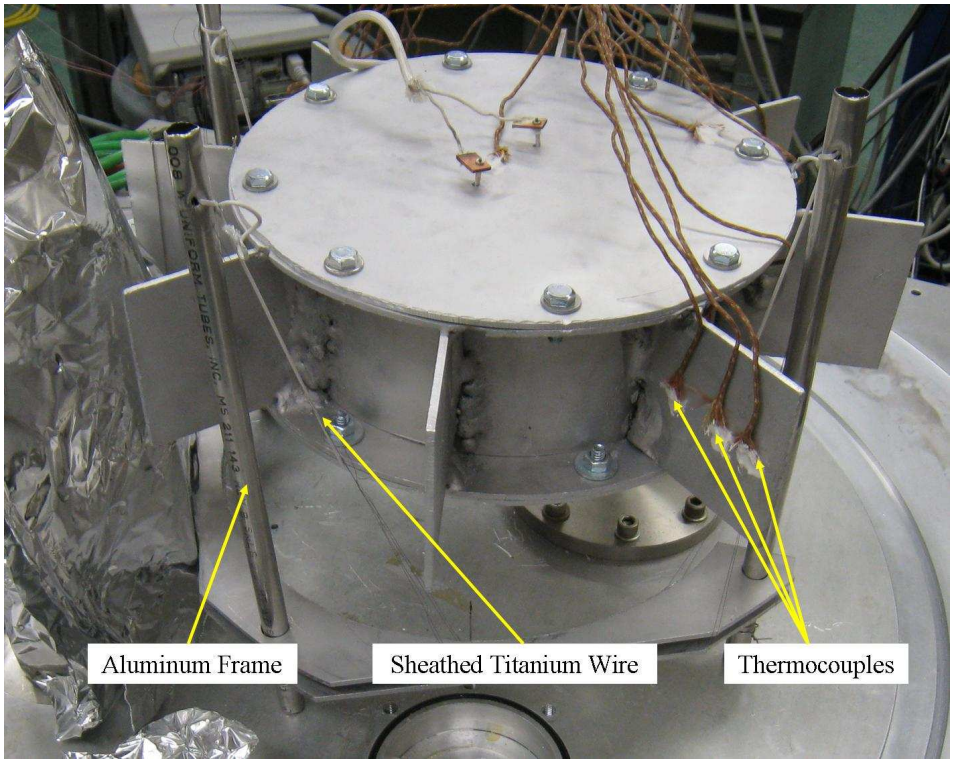

Figure 8. S-GPHS-RTG-2 experimental setup

The S-GPHS-RTG-1 utilized Omega 700 High Temperature adhesive to hold internal structures together. This adhesive proved to be very difficult to work with, as it required long curing times and was extremely brittle. The thermal cycling of multiple tests often required the interior of the S-GPHS-RTG-1 to be reconstructed between tests.

For attaching the internal components of the S-GPHS-RTG-2, CC High Temp adhesive from Omega was used. It is a silica based adhesive which proved to be much more resilient and dependable than the Omega 700 adhesive used in the 2008 ARC tests. This is primarily because its coefficient of thermal expansion is almost an order of magnitude lower, thereby allowing components to remain attached through multiple heating and cooling cycles. This resilience was best demonstrated by the fact that while the 2008 ARC tests were plagued by internal component failures, the 2009 ARC tests didn't experience one broken component in six individual tests.

The primary difference between the two series of tests, aside from the significant design changes, was the insulation packages used. The S-GPHS-RTG-1 utilized various MLI's, while the S-GPHS-RTG-2 utilized aerogel-based insulations.

MLI insulates by placing multiple foils, separated by spacers to prevent conductive heat transfer, in the path of the radiation. The thermal radiation is blocked by these foils and reradiated, with approximately half being returned in the direction of the source. Adding more layers of foil increases the MLI's insulating ability. These insulations have been used in previous RTG systems, as well as diverse space and cryogenic applications.

Because Mylar and silk, traditional cryogenic MLI materials, would be effectively destroyed around 200˚C, it was decided to use a combination of aluminum foil and fiberglass mat to construct the MLI for the S-GPHS-RTG-1. Temperatures were not expected to reach the melting point of either material.

After the first test, it became evident that the combination of aluminum and fiberglass could not withstand the high temperatures. Upon dismantling the MMRTG, the

aluminum was found to be so heavily damaged that it crumbled to the touch and appeared to have been burnt.

The assumed cause of this damage is oxidation caused by gasses released from a binder within the fiberglass mat at high temperatures. Other evidence of oxidation was the condition of the staples keeping the MLI together. They were coated by a heavy crust not seen in any other tests. Along with the destroyed MLI, all of the thermocouples within the MMRTG had heavily damaged insulation. Because of the condition of the fiberglass mat in the MLI and the fiberglass sheathing of the thermocouples, we were led to believe that fiberglass simply cannot withstand such high temperatures.

Therefore, it was decided that the MLI would be constructed of the silica fabric and stainless steel foil that would not react with it. Once again, because of a lack of materials, silica fiber insulation was used between the shoes and the shell. This insulation combination did not fail, and seemed to have worked well.

S-GPHS-RTG-1		
	Test #1	**Test #2**
Insulation Type	MLI	MLI/ Silica Fiber
Test Power	250W	250W

Table 1. S-GPHS-RTG-1 Test Matrix

The S-GPHS-RTG-2 tests made use of a silica-based aerogel. Samples of several different types of these insulations were provided by Cabot, Thermablok, and Aspen Aerogels. The sample from Cabot was granular, while Thermablok and Aspen Aerogels provided a blanket form of the insulation. For the initial set of tests, it was decided for the initial set of tests to use the granular Cabot aerogel in the spaces between the graphite shoes of the model TEC's and the interior radius of the aluminum shell, while 2 layers of

the 5mm thick Thermablok blanket were used to insulate the top and bottom of the model GPHS. While the Aspen Aerogel blankets may have performed better at high temperatures, because they were designed to operate there, than the Thermablok blankets, the samples provided were far too small to insulate the S-GPHS-RTG, and budgetary constraints prevented purchasing the amount needed for testing. After the initial tests, the device was tested with only Thermablok blankets beneath the GPHS to keep it from resting on the aluminum bottom of the S-GPHS-RTG. This test provided enough information to characterize the thermal conductivity of the Thermablok blankets. The third test series used the Cabot insulation throughout the entire interior of the S-GPHS-RTG. A fourth series of tests utilized only the Thermablok aerogel blankets.

Both types of aerogel had been treated with a hydrophobic chemical to prevent them from absorbing water from non-dry air. At high temperatures, it was feared that these chemicals could create a problem with the vacuum by outgassing. To deal with this, all of the materials were heat cleaned in excess of 300˚C for at least an hour. While this exposed the aerogel to moist air, any absorbed water was expected to outgas as the vacuum was pumped down.

A potential issue existed with the Cabot granular aerogel because it is partially transparent. This could allow thermal radiation to pass through without interacting with the insulation, carrying heat away with it. If this were allowed to happen, the insulation's effect on the device's performance would be greatly negated due to the dominance of thermal radiation. To prevent thermal radiation from passing through, graphite powder was added to opacify the insulation. 13% weight percent graphite powder was added. By

opacifying the aerogel, the thermal radiation will interact within the insulation, transferring its energy and capturing the heat in the insulation.

In order to contain the granular aerogel, all gaps between the graphite plates of the model TEC's were sealed using the Omega CC High Temp adhesive. For the second series of tests, which utilized only granular aerogel, woven silica blankets were used on the top and bottom of the GPHS to keep the insulation from filling the void between the GPHS and the graphite plates.

S-GPHS-RTG-2						
	Test #1	**Test #2**	**Test #3**	**Test #4**	**Test #5**	**Test #6**
Insulation Type	Cabot/ Thermablok Aerogels	Cabot/ Thermablok Aerogels	None	Cabot Aerogel	Cabot Aerogel	Thermablok Aerogel
Test Power	250W	250W	250W	250W	250W	250W

Table 2. S-GPHS-RTG-2 Test Matrix

In both series of testing, temperature data was gathered via thermocouples located at various places on and within the S-GPHS-RTG. Thermocouple locations used in the different tests were similar but not identical because of design changes. All of the thermocouples used in the experiments were Type K Omega thermocouples. The uncertainty associated with Type K thermocouples is the greater of either ±2.2˚C or ±0.75% of the reported value. [10] For the purposes of the data collected in this study, the uncertainty from a thermocouple never exceeded 5˚C.

The first S-GPHS-RTG-1 test utilized 17 thermocouples located throughout the MMRTG. Later S-GPHS-RTG-1 tests utilized only nine thermocouples. Fewer thermocouples were used because of damage to the insulation of the eight internal thermocouples in the first test. However, enough thermocouples remained to gather relevant data from the second test. The redundancy of initially using 17 thermocouples

proved to be well planned. All thermocouples were insulated by woven fiberglass sheaths.

Twelve fiberglass sheathed thermocouples made measurements of the exterior portions of the S-GPHS-RTG shell. Another such thermocouple was attached to the cryocooler present in the vacuum chamber to make sure it remained undamaged. These thermocouple junctions were also welded, as high temperatures (above the melting point of solder) could not be ruled out. For the interior temperature measurements of the GPHS and graphite plates, Omega's "OMEGACLAD XL Thermocouple Probes" were used. These probes were deemed necessary because the internal temperatures observed in 2008 ARC tests destroyed the same fiberglass sheathing used by the thermocouples on the exterior of the S-GPHS-RTG. All of the thermocouples were held in place with Omega CC High Temp adhesive.

During testing, it was found that one of the internal thermocouples adhered to the model GPHS was malfunctioning. Its behavior implied that it was disconnected somewhere, likely the feed-through into the vacuum chamber. Because of the time that would have been required to fix this and the fact that a redundant thermocouple located on the model GPHS was functioning properly, it was simply ignored.

Table 3 lists the number of thermocouples used in different locations. Figures 9, 10, 11, and 12 map the locations of these thermocouples. These locations are marked with red circles. Not all marked locations are applicable to every test.

Location	Thermocouple Numbers							
	S-GPHS-RTG-1		S-GPHS-RTG-2					
	Test #1	Test #2	Test #1	Test #2	Test #3	Test #4	Test #5	Test #6
GPHS	1-4	1	1	N/A	1	1	1	1
TEC Graphite	5-6	5	5	5	5	5	5	5
TEC Tungsten	7-8	N/A	N/A	N/A	N/A	N/A	N/A	N/A
Shell	9	9	9	9	N/A	9-10	9-10	9-10
Cooling Fins	11-13	11-14	11-13	11-13	11	11-14	11-14	11-14
Top of Device	15-17	15	15-16	15-16	15-16	15-16	15-16	15-16
Bottom of Device	18-19	18	18	18	18	18-19	18-19	18-19
Total # of TC's	**17**	**9**	**9**	**8**	**7**	**13**	**13**	**13**

Table 3. Thermocouple locations

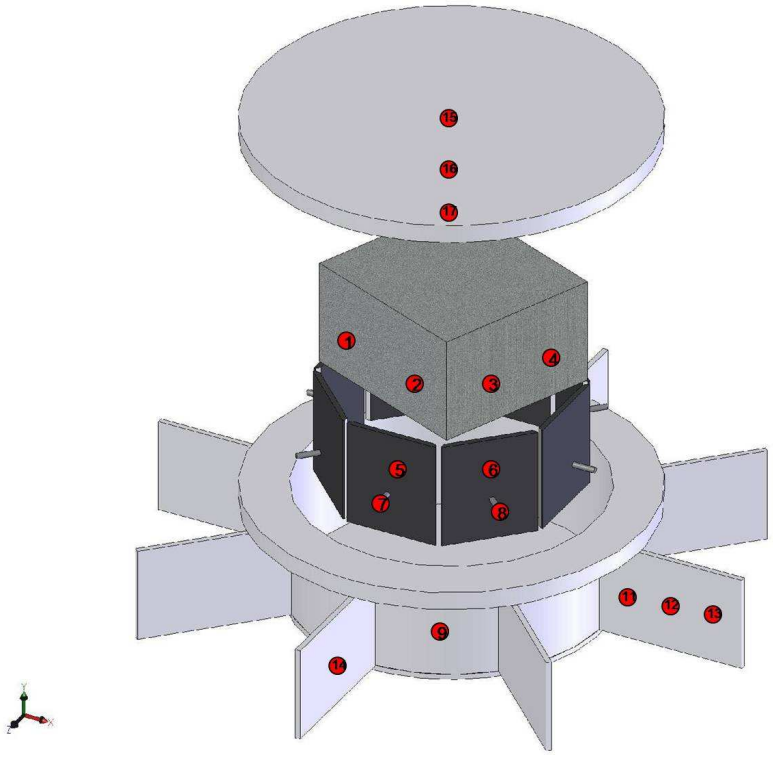

Figure 9. Thermocouple locations on the S-GPHS-RTG-1

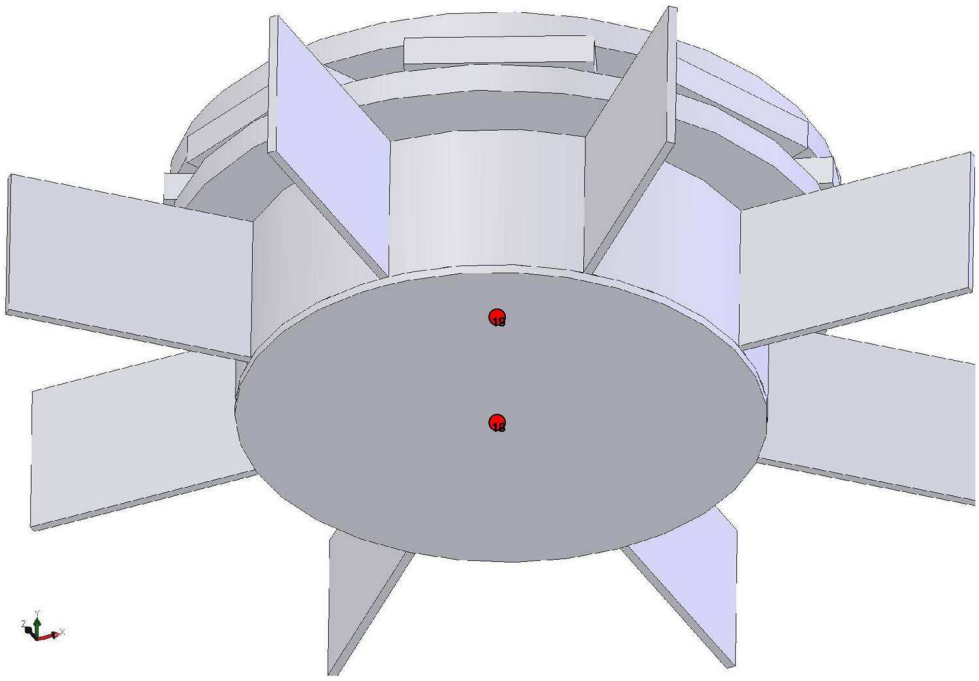

Figure 10. Thermocouple locations on the S-GPHS-RTG-1

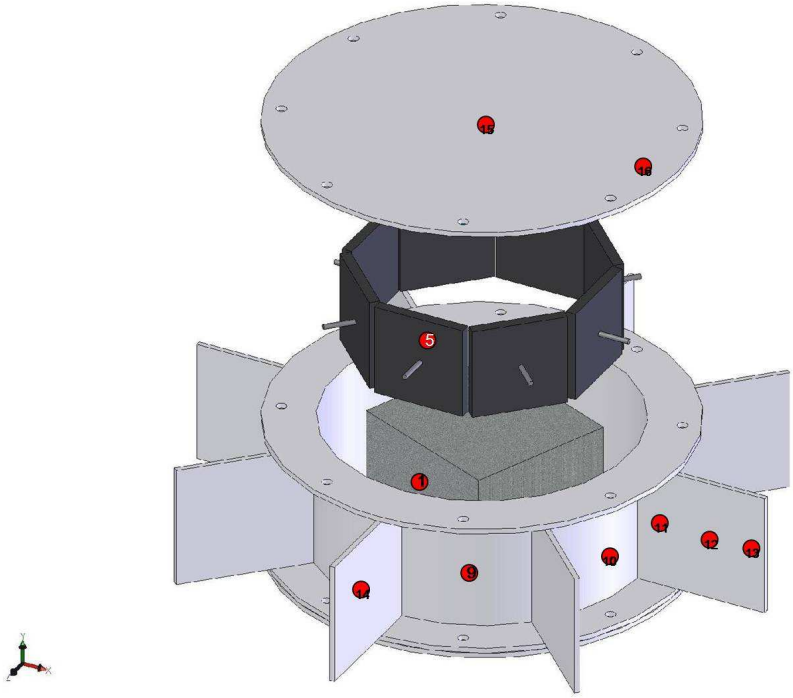

Figure 11. Thermocouple locations on the S-GPHS-RTG-2

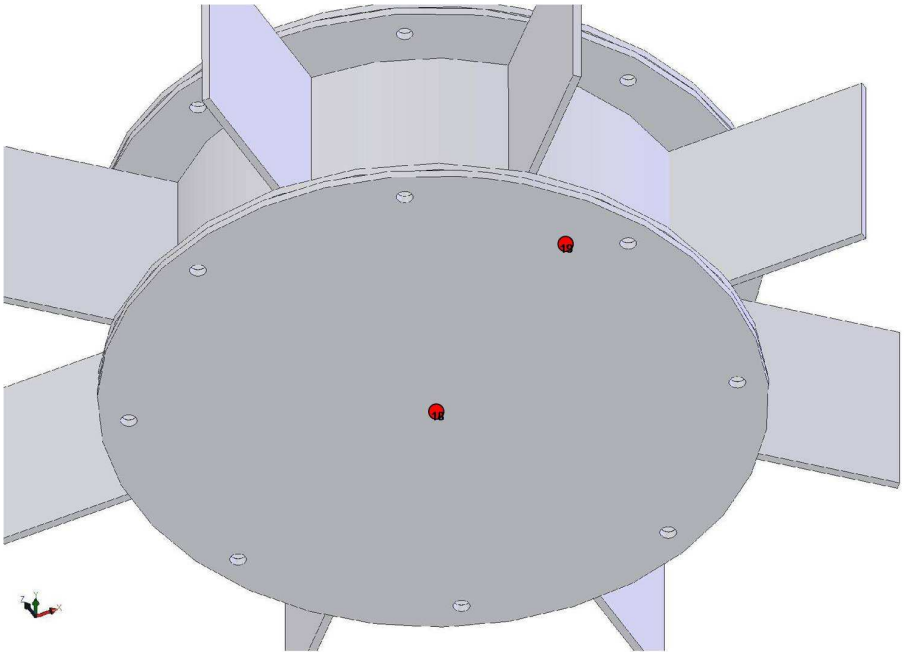

Figure 12. Thermocouple locations on the S-GPHS-RTG-2

The temperature of the GPHS was measured on vertical faces which radiated heat out to the TEC's. After the first S-GPHS-RTG-1 test, it was determined that temperatures were nearly uniform on the GPHS faces and only one measurement needed to be taken. The temperatures of the TEC Graphite were taken on the interior faces which received radiation. Temperature recording of the TEC tungsten was deemed to be questionable at best and was, therefore, discontinued. Shell temperatures were recorded centrally between the top, bottom, and two cooling fins on the shell's exterior face. The cooling fin thermocouples recorded temperatures at three evenly-spaced radial distances. The temperatures on the top of the S-GPHS-RTG were recorded at the center point for each test, and at increasing radii if extra thermocouples were available. The locations on the bottom were selected in a similar fashion.

All of the thermocouples were attached using whichever adhesive was used in the construction of the device.

Power was supplied to the model GPHS by an HP 6575A DC Power Supply. Two wires were attached to two small copper plates with holes drilled in them. The copper plates were attached to the model GPHS's threaded leads using small nuts. Because the short circuit in the model GPHS was approximately 60 times more resistant than the main heater, it was deemed to be of minimal concern.

Temperature data was gathered by an Agilent 34970A 20 channel multiplexer, which was controlled by a PC running LabVIEW that logged the data. The data was then analyzed using Microsoft Excel.

Besides the physical experiments, part of the goal of this study was to create a computational model of the S-GPHS-RTG in Thermal Desktop. The hope is that an accurate model may relieve the need for physical experiments. A simple 3D model of the S-GPHS-RTG was first constructed in AutoCAD Mechanical. Thermal Desktop then utilized this model, along with physical parameters which were supplied. This model included the GPHS, the shell, and the components of the TEC's, but neglected the insulation. Once this was built, a large structure that was approximately the size of the vacuum chamber was created around the S-GPHS-RTG. Separate models were built for both the S-GPHS-RTG-1 and the S-GPHS-RTG-2 at the time of their physical tests.

Material properties were then assigned to the different parts of the model. These properties included density, thermal conductivity, heat capacity, and emissivity. Many of these values are difficult to locate and identify for specific materials, so in some cases a closely related surrogate is used as the best approximation. In the case of the S-GPHS-

RTG’s shell, Aluminum 2024 T6 was used instead of Aluminum 6061 T6 because a more complete set of properties could be found over a wider temperature range. The model GPHS was also approximated as a solid block of graphite. The emissivity of graphite was assumed to be 1 because it is pure carbon, while the emissivities of aluminum and tungsten were assigned to be 0.69 and 0.84, respectively.

The thermal conductivity of the aerogel insulation used a single set of values that were approximated from literature provided by the manufacturers of the aerogel insulation. Because previous experimentation had indicated the thermal conductivity of silica aerogel to be approximately ~5/8 of its original value when placed in vacuum conditions similar to those expected for these tests[7], this factor was applied. The doping of the granular aerogel with graphite was also expected to change the thermal conductivity. To approximate this doping, the thermal conductivity of the aerogel was approximated to be 90% aerogel and 10% graphite. The known values were then plotted and a curve was fit which allowed higher temperature values to be extrapolated, see Figure 13. With relation to the available literature on the thermal conductivity of silica aerogels, these values were assumed to be conservative. Table 4 lists the material data used in the Thermal Desktop models. [11 12 13]

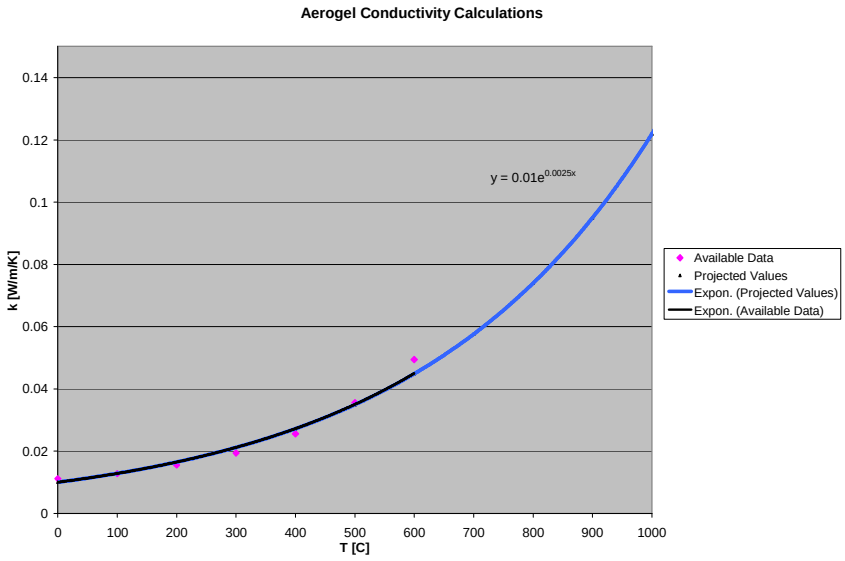

Figure 13. Aerogel thermal conductivity values used in Thermal Desktop calculations

Material	Temp [C]	k [W/m/K]	C_p [J/kg/K]	ρ [kg/m^3]
CC High Temp	260	1.3845	N/A	2260
Aerogel Insulation	0	0.17998	N/A	180
	100	0.19199		
	200	0.20565		
	300	0.221		
	400	0.239		
	500	0.261449		
	600	0.28873		
	700	0.3105		
	800	0.34125		
	900	0.37714		
	1000	0.41945		
Aluminum 2024 T6	-173.15	65	473	2770
	-73.15	163	787	
	126.85	186	925	
	326.85	186	1042	
Graphite	N/A	130	750	1720
Tungsten	-173.15	208	87	19300
	-73.15	186	122	
	126.85	159	137	
	326.85	137	142	
	526.85	125	145	
	726.85	118	148	
	926.85	113	152	
	1226.85	107	157	
	1726.85	100	167	
	2226.85	95	176	

Table 4. Material Properties used in Thermal Desktop calculations [11 12 13]

In order to simulate the thermal radiation occurring in the model, Thermal Desktop runs a Monte Carlo simulation from the activated surfaces. In order for a surface to transmit or receive thermal radiation in the model, it must be activated by the user and have its emissive properties defined. For the models of the S-GPHS-RTG that included insulation, the interior faces of the TEC octagon, all faces except the top and bottom of the GPHS, all external faces of the S-GPHSRTG shell, and all surfaces of the vacuum

chamber were activated for radiation. For the tests that did not include insulation all surfaces were activated, with the sole exception being the bottom face of the GPHS as it rested firmly on insulation.

The external faces of the vacuum chamber were also defined as experiencing natural convection, as would be expected. The vacuum chamber is modeled as a flat disc on the bottom with cylindrical walls and a hemispherical top. The bottom was modeled as a horizontal plate heated from the top with the sides and top modeled as vertical cylinders, which is as near an approximation as possible for the hemispherical top. These were all modeled using the "Contactor" feature which linked the surfaces to a node. This node was set as a boundary condition at room temperature.

The heat loads were applied to the surface of the GPHS. The application of the heat load to the surface rather than the center of the GPHS was deemed an appropriate approximation because applying the heat to the center revealed that no major temperature gradients exist on the GPHS. Applying the heat to the center made the temperature gradient maps difficult to understand because the center of the GPHS would be hundreds of degrees warmer than the rest of the GPHS, skewing the color scale.

Because some previous data for the S-GPHS-1's behavior in atmospheric conditions existed, convective heat mechanisms were activated throughout the device and the results were compared to physical data. Holding the temperature of the GPHS at a constant 410˚C, the temperatures seen in the original OSU tests, the model was tuned until all of the elements were within 10˚C of the temperatures observed during the OSU tests. At that point, the constant temperature of the block was removed, and a heat load of 250W_t was added. After this heat load was added, all temperatures remained within 35˚C, and the

model was assumed to be relatively accurate. It is also worth noting that for the purposes of building this model, the material properties of the insulation used in the OSU experiment were used. Table 5 lists the temperatures observed in the 2006 OSU tests and the Thermal Desktop model. The values listed for the Thermal Desktop are ranges because of the inexact nature of the regions. Figures 14 and 15 illustrate the Thermal Desktop model that was tuned to these results.

S-GPHS-RTG-1 Ambient Atmosphere Tests			
Location	**Test #1 (˚C)**	**Test #2 (˚C)**	**Thermal Desktop (˚C)**
Top Plate, Center	177.5	177.5	171.5-177.1
Top Plate, Edge	173.1	173.1	165.9-171.5
Bottom Plate, Center	154.5	155.9	154.8-149.3
Bottom Plate, Edge	148	148.7	143.7-149.3
Shell	145.2	146.5	138.1-143.7
Fin, Interior	140.2	141.6	138.1-143.7
Fin, Middle	133	133.7	127-132.6
Fin, Exterior	122.5	120.7	127-132.6
TEC Graphite	326.7	326.7	271.7-294.7
GPHS	409.5	409.1	386.9-410

Table 5. Steady state temperatures of ambient atmosphere S-GPHS-RTG-1 tests[6]

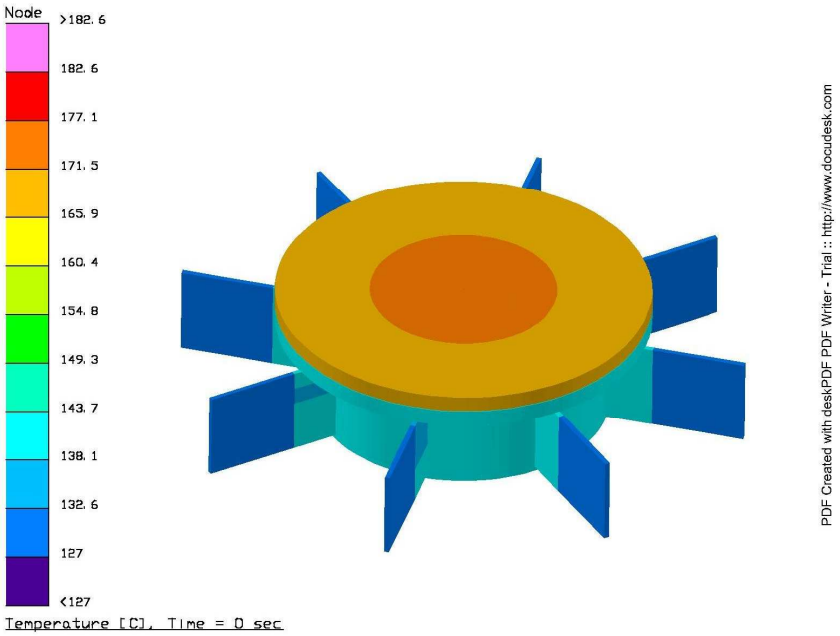

Figure 14. Thermal Desktop results for external components of 2006 OSU testing

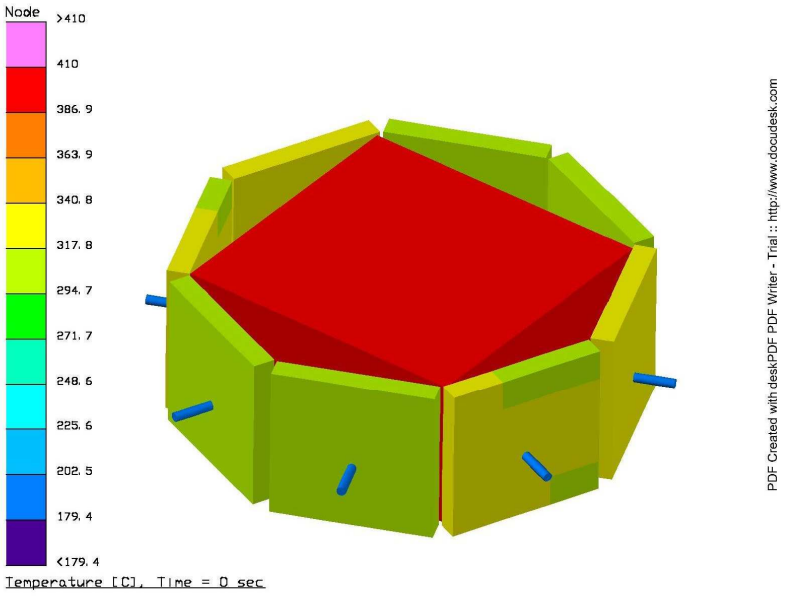

Figure 15. Thermal Desktop results for internal components of 2006 OSU testing

This model was then used to help approximate the conditions that would be experienced during the vacuum testing of the S-GPHS-RTG-1. Because the performance of the insulation used for the vacuum testing was not definitively known, a perfect insulator, k=0 W/m/K, was used to find the maximum internal temperature that could be reached during the physical testing.

Because the S-GPHS-RTG-2 had not been previously tested, the model was simply set up and allowed to run with the provided material properties. The results of these computations were unexpectedly high temperatures. The high temperatures in the model were cause for some concern and suspicion.

5. TEST RESULTS

As previously mentioned, the insulation failed dramatically in the first S-GPHS-RTG-1 test. Based on the observed data, the insulation failed as the temperatures were still rising, and allowed the temperatures to drop before stabilizing.

These temperatures, however, should be viewed skeptically for two reasons. The first is that the components never reached a steady state temperature. Because many of the components heat at different rates, none of the temperature gradients between these components can be compared to tests which were able to reach steady state. The second reason is that the insulation failed by oxidation, likely an exothermic reaction which may have led to increased heat production within the S-GPHS-RTG-1. This added heat may have artificially raised temperatures. Because of this, the results of this test will be ignored, for the most part, in the remainder of this study. Table 6 lists the temperatures that were reached in the first test of the S-GPHS-RTG-1. Figure 16 shows a photograph of the damaged MLI.

Thermocouple Location	Temperature [C]
Top Plate, Center	193
Top Plate, Center Interior	201
Top Plate, Center Edge	175
Shell, Middle	238
Left Fin, Interior	236
Left Fin, Middle	214
Left Fin, Exterior	194
Bottom Plate, Center	221
Bottom Plate, Center Edge	237
GPHS 1	603
GPHS 2	602
GPHS 3	593
GPHS 4	591
Graphite Shoe 1	589
Graphite Shoe 2	593
Tungsten Rod 1	438
Tungsten Rod 2	444
Power	258.75W

Table 6. Maximum temperatures of S-GPHS-RTG-1 test using MLI

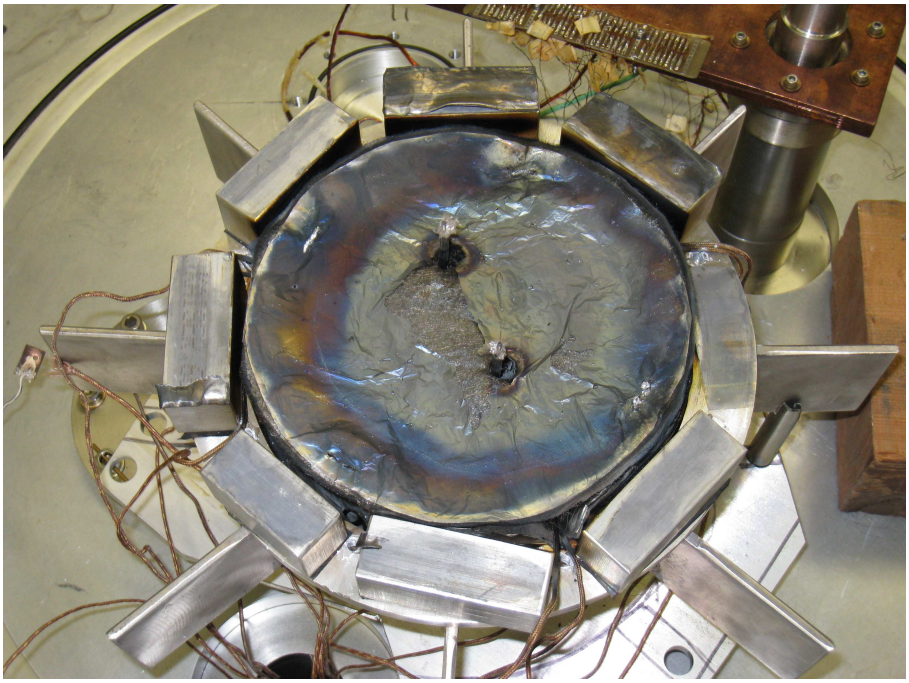

Figure 16. Photograph of damaged MLI from S-GPHS-RTG-1 Test #1

Between the first and second S-GPHS-RTG-1 tests, a quick, full power test was run without thermocouples. The test used silica fiber insulation and its sole purpose was to verify that the insulation wouldn't fail at high temperatures. Because the test was only oriented at confirming the silica insulation's ability to survive and the model TEC's were not included, it was deemed unnecessary to gather temperature data. The test yielded encouraging results as the insulation remained intact.

The second test did not reach internal temperatures as high as the first test. While the specific cause of this variation is not entirely understood, it is assumed to be related to three possible causes. The first is the use of stainless steel instead of aluminum in the MLI. The second is better thermal contact between the GPHS and the bottom of the shell. Lastly, silica fiber insulation was used instead of MLI between the graphite shoes and the interior of the shell. This insulation is expected to have a higher thermal conductivity than MLI, which could not be used due to timing and material factors.

Thermocouple Location	**Temperature [C]**
Top Plate, Center	233
Bottom, Center	223
Left Fin, Interior	218
Left Fin, Middle	205
Left Fin, Exterior	193
Shell	222
Right Fin, Middle	201
GPHS	589
Graphite Shoe	572
Power	260.2W

Table 7. Steady state temperatures of S-GPHS-RTG-1 tests using MLI/silica fiber

Transient temperature data was gathered as the device heated up to provide insight into its behavior. This transient data was only used to monitor the heating behavior and not used for analysis. When the insulation failed, the transient data did not follow the smooth curve that is indicated by the second test's data. While that data has been lost due to a computer recording error, it indicated that the temperatures rose to a point where the insulation presumably failed and then began to drop steadily. The second test's transient data, however shows a very smooth warming curve which indicates that no insulation failure occurred. The small ledges on the leading edge of the curve in the second test's transient data were the result of some offgassing which required interruption of the electrical power.

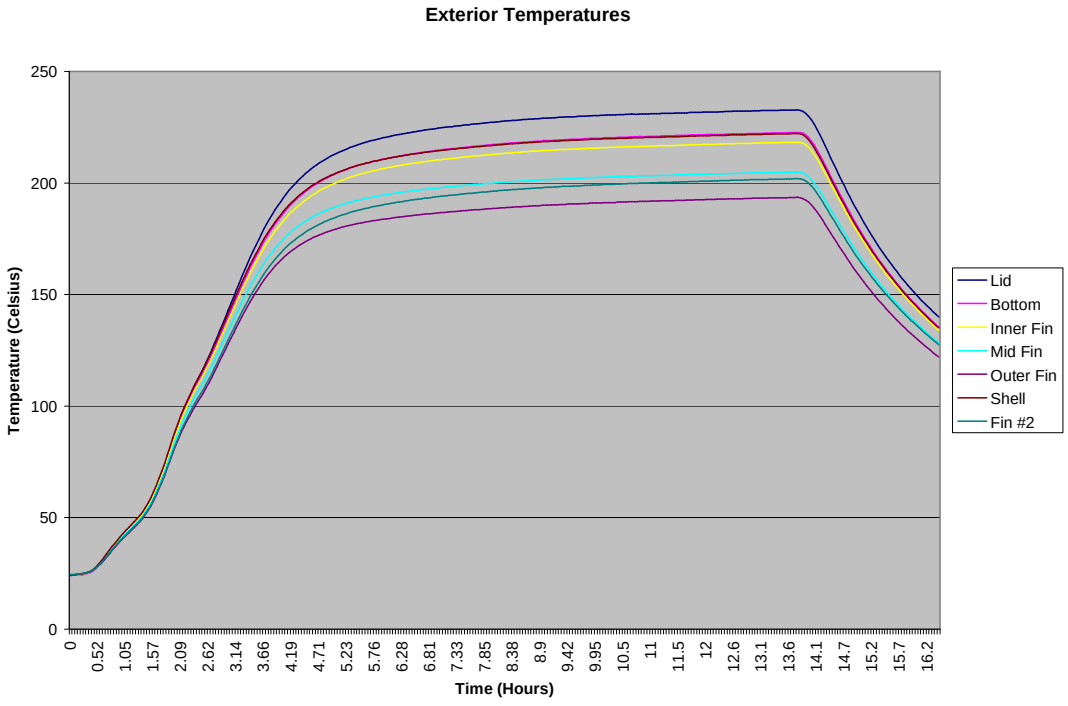

Figure 17. Transient temperatures of S-GPHS-RTG-1 external components using MLI/silica fiber

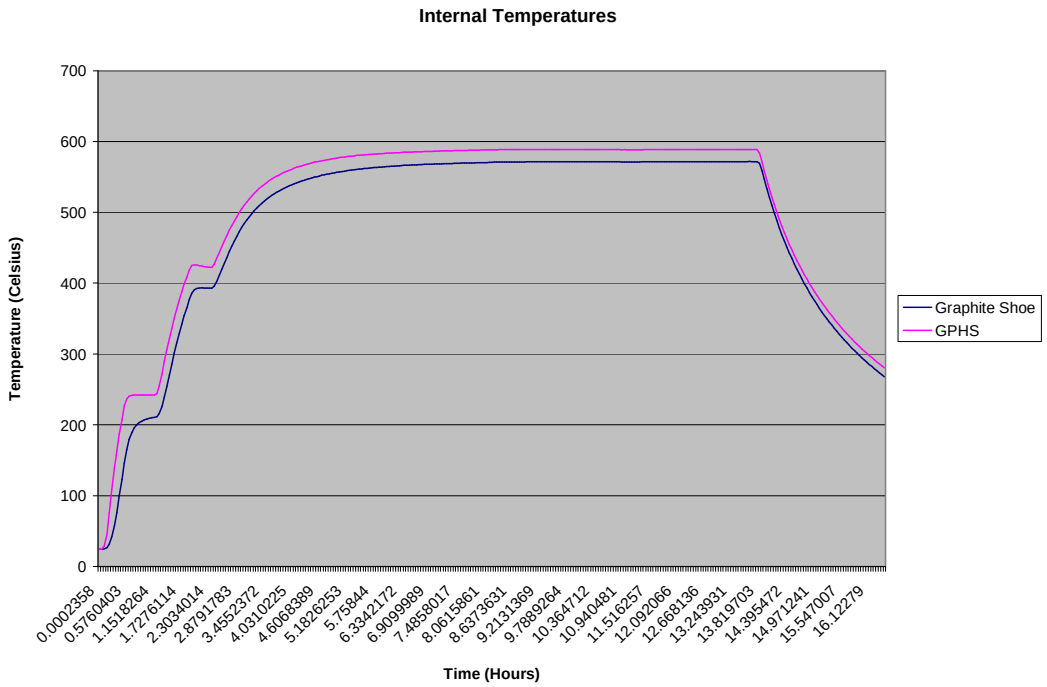

Figure 18. Transient temperatures of S-GPHS-RTG-1 external components using MLI/silica fiber

The first series of tests used the Thermablok blankets above and below the GPHS and the opacified Cabot aerogel between the graphite of the TEC's and the S-GPHS-RTG's shell. Because the temperatures were expected to be significantly higher than the insulation had previously been tested, the power was not immediately increased to full power in order to observe any unexpected occurrences. Aside from some minor outgassing, the pressure never rose above 4 milliTorr and no such occurrences were observed. The power was started at ~50W_e, allowed to reach steady state, then increased to ~125W_e until steady state was again reached, and was then finally increased to ~250W_e.

It is worth noting that because of small inconsistencies with the power supply, minor variances were seen in power levels throughout testing. These variances were monitored

and corrected when deemed necessary. Power levels stayed within ±5 W, with the exception of the final S-GPHS-RTG-2 test which reached nearly 273 W due to being run overnight without observation, as discussed later. For the purposes of the remainder of this paper, all tests were conducted at full power, approximately 250W.

As can be seen in Table 8, the redesigned S-GPHS-RTG-2, using a combination of aerogel insulations was unable to reach the steady state temperatures that were observed in the 2008 ARC testing. This was unexpected, as the aerogel insulations were ubiquitously thought to be superior insulators. However, a direct comparison of the insulating abilities of MLI and aerogel is difficult to obtain because of the different mechanisms of heat transfer as well as different surface contact that they experience with components. Because of this revelation, different possible causes were investigated. As the S-GPHS-RTG-2 cooled, the pressure remained constant. The cooling of the very hot device would be expected to decrease the pressure inside the vacuum chamber, so all seals were double checked and three o-rings were found to be defective.

The o-rings were replaced, and the S-GPHS-RTG-2 was quickly retested. While the temperatures did increase, they did not increase to the expected level.

Upon dismantling the S-GPHS-RTG-2 it was observed that the Thermablok blankets appeared charred. While it is unknown what effect this had on the device's temperatures, it is presumed to not be favorable.

As discussed earlier, S-GPHS-RTG-2 did experience lower external surface temperatures than the S-GPHS-RTG-1. This difference is likely explained by the increased overall size and surface area available for radiating heat to the environment.

Thermocouple Location	Temperature [C]	
	Test #1	**Test #2**
GPHS	547.37	N/A
TEC Graphite #1	521.97	544.19
Shell #1	184.76	181.74
Fin #1 End	179.57	177.79
Fin #1 Midpoint	184.93	184.64
Fin #1 Inside	185.51	183.37
Fin #2 Midpoint	N/A	N/A
Top Center	194.87	190.35
Top Edge	180	171.6
Bottom Center	181.87	180
Power	248.6W	250.7W

Table 8. Steady state temperatures of S-GPHS-RTG-2 tests using Cabot/Thermablok aerogel

The second set of tests was intended to merely act as a control. It was expected that because the test was less complex, it would be easier to model in Thermal Desktop for model confirmation. However, as the test was being conducted, it was noted that the thermal conductivity of the Thermablok blanket could be inferred from the observed temperature gradients. Prior to the test being sealed within the vacuum chamber, a thermocouple was placed beneath the Thermablok blanket that the model GPHS rested on. Thermocouples provided temperature information for the GPHS, graphite plates, lid and bottom of the aerogel blanket. Most of the other thermocouples had become detached, and because of a lack of adhesive, they had to remain in that condition.

Assuming that the temperature of the surface of the model GPHS was homogeneous, the sides radiated heat entirely to the graphite of the TEC's, the top face radiated heat entirely to the lid of the S-GPHS-RTG's shell, and the only other method of heat transfer

was through the Thermablok blanket, all heat loss from the model GPHS could be accounted for. The amount of heat being released from the model GPHS is strictly controlled by the power supply. Because the thickness of the blanket, area of heat transfer, and temperature gradient over the blanket were all known, in addition to the amount of heat flowing, the thermal conductivity, k, can be easily calculated.

$$\dot{Q}_{Tot} = 250\ W \tag{1}$$

$$\dot{Q}_{Tot} = \dot{Q}_{Rad} + \dot{Q}_{Cond} \tag{2}$$

$$\dot{Q}_{Rad} = (2A_{L\times H} + 2A_{W\times H})\varepsilon\sigma\,(T_{GPHS}^{4} - T_{Graphite}^{4}) + A_{L\times W}\varepsilon\sigma\,(T_{GPHS}^{4} - T_{Al}^{4}) \tag{3}$$

$$\dot{Q}_{Cond} = \frac{A\times k}{L}(T_{GPHS} - T_{Bottom}) \tag{4}$$

Thermocouple Location	Temperature [C]
	Test #3
GPHS	362.70
TEC Graphite #1	343.48
TEC Graphite #2	345.54
Fin #2 Midpoint	179.55
Top Center	190.08
Top Edge	169.47
Bottom Center	241.02
Power	249.17W

Table 9. Steady state temperatures of uninsulated S-GPHS-RTG-2

A simple C++ script was written to calculate k. As part of that calculation, all temperatures were converted from Celsius to Kelvin. The calculated value of k for the Thermablok blanket with the model GPHS at a temperature of 362˚C was 1.827 W/m/K, with a calculated error of ±0.0849 W/m/K. [14] This error is a result of the measurement uncertainties associated with the thermocouples.

Ideally this number, which is significantly larger than those used in the Thermal Desktop model, could be incorporated into the computer model. However, by the time this conductivity was measured, the software's license had expired.

The first series of tests were initially planned to use Cabot's granular aerogel for all of the insulation, but used Thermablok blankets on the top and bottom of the model GPHS because of a limited supply of Cabot insulation. For the third series of tests, we were able to obtain more granular aerogel. After heat cleaning this aerogel and doping it with the same amount of graphite powder as in previous tests, it was incorporated to insulate the top and bottom of the model GPHS. More Omega CC High Temp adhesive was also obtained, allowing for all external thermocouples, with the exception of one malfunctioning thermocouple, to be reattached.

These tests were again disappointing, failing to reach even the temperatures achieved in the first tests by a wide margin. A small short circuit was suspected during the fourth test, and was fixed for the fifth test, resulting in slightly higher temperatures.

Thermocouple Location	Temperature [C]	
	Test #4	**Test #5**
GPHS	511.15	519.91
TEC Graphite #1	502.37	511.67
TEC Graphite #2	501.78	511.25
Shell #1	176.07	180.75
Shell #2	175.15	179.10
Fin #1 Inside	172.18	175.83
Fin #2 End	161.62	164.64
Fin #2 Midpoint	167.59	170.54
Fin #2 Inside	173.04	176.81
Top Center	189.26	188.11
Top Edge	180.92	179.56
Bottom Center	178.96	182.17
Bottom Edge	160.49	161.42
Power	246.0W	251.3W

Table 10. Steady state temperatures of S-GPHS-RTG-2 tests using Cabot aerogel

The tests utilizing only Cabot's granular aerogel reached lower temperatures than the first tests, inferring that the Thermablok blanket may be the superior insulation material. While this was contrary to initial expectations, a test was composed using only Thermablok blankets as insulation to test this idea. Two strips were cut and fitted between the graphite of the TEC's and S-GPHS-RTG's shell. This gave 1 cm of Thermablok insulation at all locations where insulation was present.

This all-Thermablok insulation package did give much better results than Cabot's granular aerogel. It is worth noting that because the test was run at a time when the power level could not be constantly observed and adjusted the final power level was 272.74W_e, almost 10% too high. While this undoubtedly raised the steady state temperatures, it was deemed to still be a relevant, comparable test.

Thermocouple Location	Temperature [C]
	Test #6
GPHS	589.37
TEC Graphite #1	584.59
TEC Graphite #2	581.20
Shell #1	188.78
Shell #2	185.53
Fin #1 Inside	181.42
Fin #2 End	171.32
Fin #2 Midpoint	177.12
Fin #2 Inside	184.00
Top Center	161.07
Top Edge	186.49
Bottom Center	159.81
Bottom Edge	155.77
Power	272.7W

Table 11. Steady state temperatures of S-GPHS-RTG-2 test using Thermablok aerogel

The temperature gradient between the base of the S-GPHS-RTG and the end of the fins is an important indicator of how well the S-GPHS-RTG radiates heat. The 2008 ARC test saw a larger fin gradient because the higher temperatures of the S-GPHS-RTG's shell experienced facilitated better radiation of waste heat.

Transient data collected for all of the tests indicated that they heated up properly and did not experience any dramatic insulation failures. It is also worth noting that none of the insulation packages allowed the internal structures of the S-GPHS-RTG to heat up significantly faster or slower.

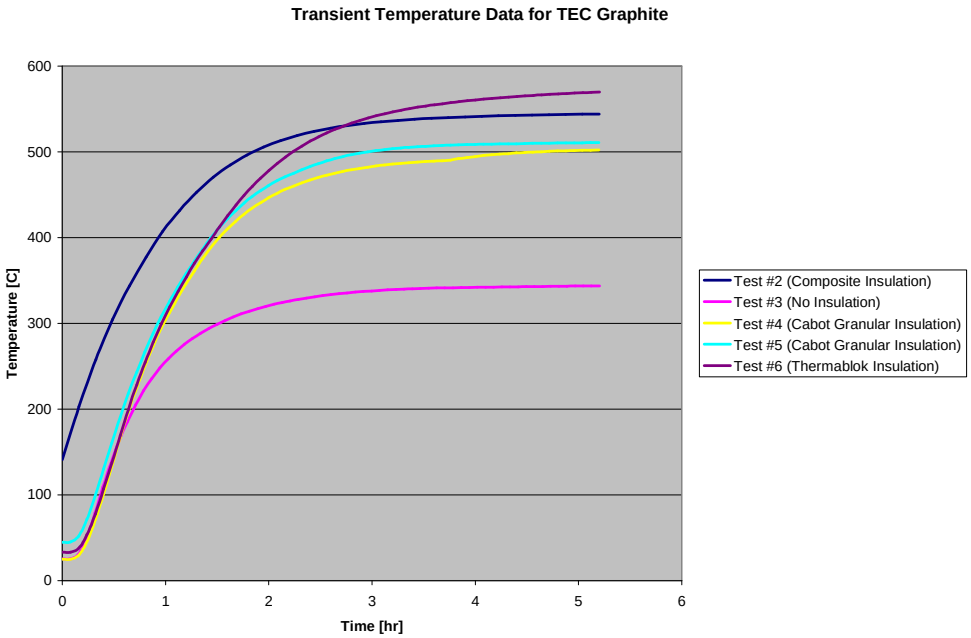

Figure 19. Transient temperatures of S-GPHS-RTG-2 TEC graphite

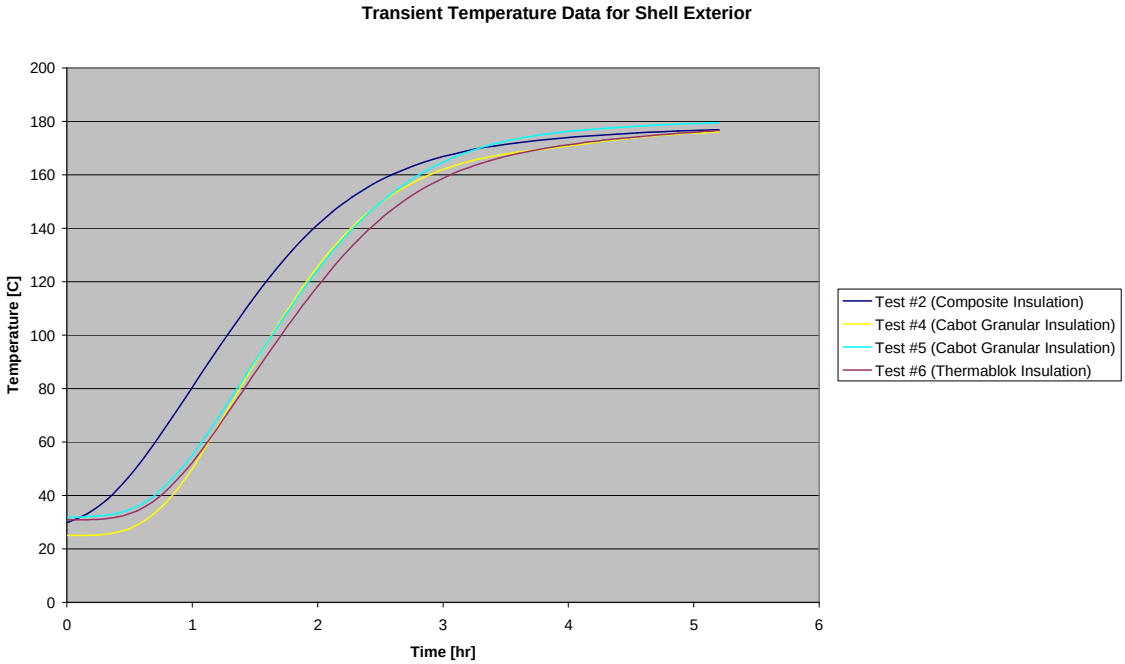

Figure 20. Transient temperatures of S-GPHS-RTG-2 shell

Tests conducted in Thermal Desktop gave different solutions than those observed in any of the tests, especially on the exterior surfaces. The temperature resolution of the computer's predictions was poor, mostly due to inexperience operating Thermal Desktop. The computer anticipated results that were both higher and lower than what were experienced in physical tests see Table 12 and Figure 21.

For the S-GPHS-RTG-1, Thermal Desktop was run with perfect insulation, k=0 W/m/K. This was because of uncertainty as to how the MLI would perform. This did, however, provide a useful upper limit of temperatures to expect, which proved useful when selecting MLI materials. Also, when the first S-GPHS-RTG-1 insulation package failed the temperatures were still climbing at an impressive rate, though this may have been a result of oxidation. Had it not failed, the resulting temperatures may have been near the computer's estimates.

Location	**Predicted Values (˚C)**
Top Plate	283-411
Bottom Plate	156-347
Shell	156-283
Fins	27-91
TEC Graphite	475-539
GPHS	539-603

Table 12. Thermal Desktop prediction of S-GPHS-RTG-1 steady state temperatures

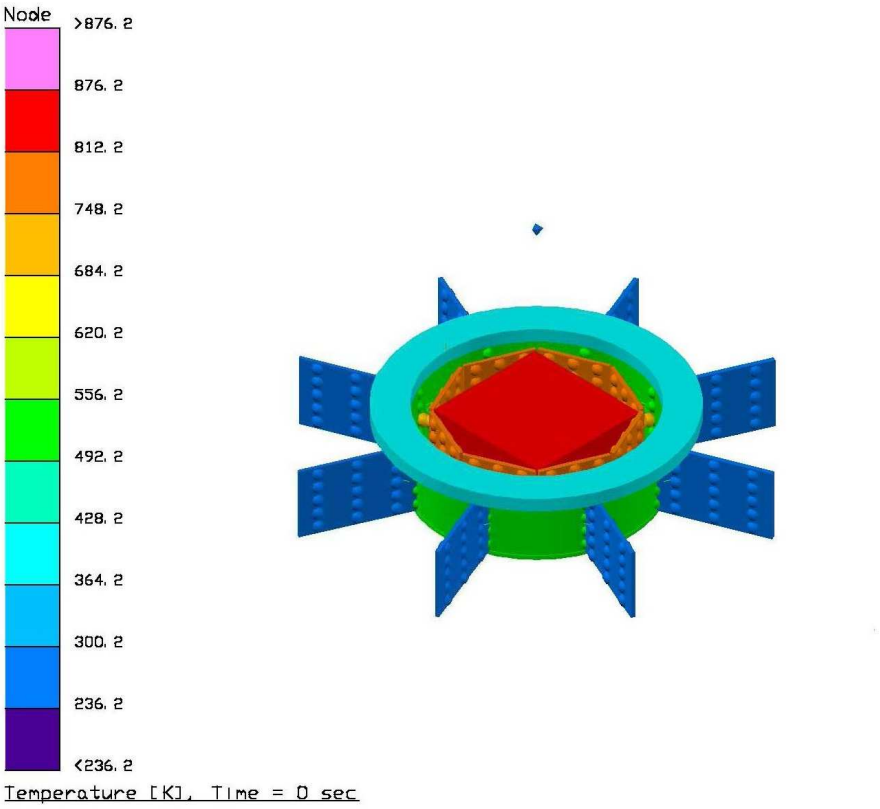

Figure 21. Thermal Desktop prediction of S-GPHS-RTG-1 steady state temperatures

The computer predictions of the S-GPHS-RTG-2's performance allowed for better temperature resolution, thanks to increased familiarity with the software. These values are listed in Table 13 and illustrated in Figures 22 and 23. The temperatures predicted for the external components of the S-GPHS-RTG-2 were also much lower than those observed in physical testing, while the predicted temperatures for internal components were much higher. These two observations indicated that the insulation used in the virtual model was much more effective than what existed in reality. Further Thermal Desktop tests using the calculated coefficient of thermal conductivity of the Thermablok insulation from the test without insulation will provide better insight into the effectiveness of the Thermal Desktop model.

Location	Predicted Values (˚C)
Top Plate	174.1-179.5
Bottom Plate	174.1-179.5
Shell	176.8-178.6
Fins	170.5-179.5
TEC Graphite	616.6-675.9
GPHS	675.9-705.6

Table 13. Thermal Desktop prediction of S-GPHS-RTG-2 steady state temperatures

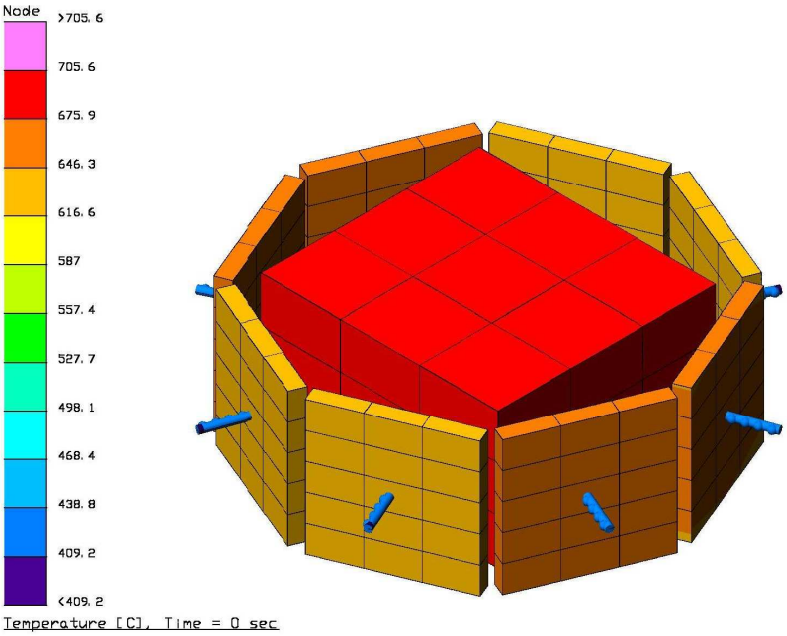

Figure 22. Thermal Desktop prediction of S-GPHS-RTG-2 internal steady state temperatures

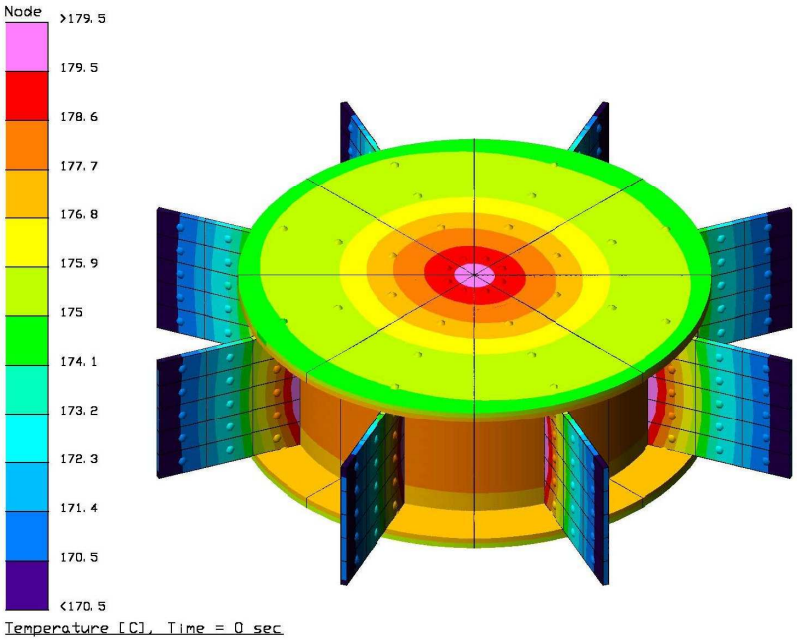

Figure 23. Thermal Desktop prediction of S-GPHS-RTG-2 external steady state temperatures

6. DISCUSSION

The results of the S-GPHS-RTG vacuum tests provided insight into the behavior of several potential insulation packages, as well as two different shell designs.

Various values can be looked at to measure the performance of the tests. The first criterion is internal temperature of the GPHS. This gives a very obvious indication of how well the insulation is performing, particularly directly above and below the GPHS. The second important value is the temperature gradient between the inner face of the graphite shoe of the TEC and the exterior of the S-GPHS-RTG shell. This is a measure of the temperature gradient that the TEC is exposed to, and since temperature gradients drive TEC performance, as discussed previously, this value is extremely important. Higher gradient values are an indication that the device will perform more efficiently. The temperature gradient over the cooling fins also provides information on how well the S-GPHS-RTG is radiating heat to the environment.

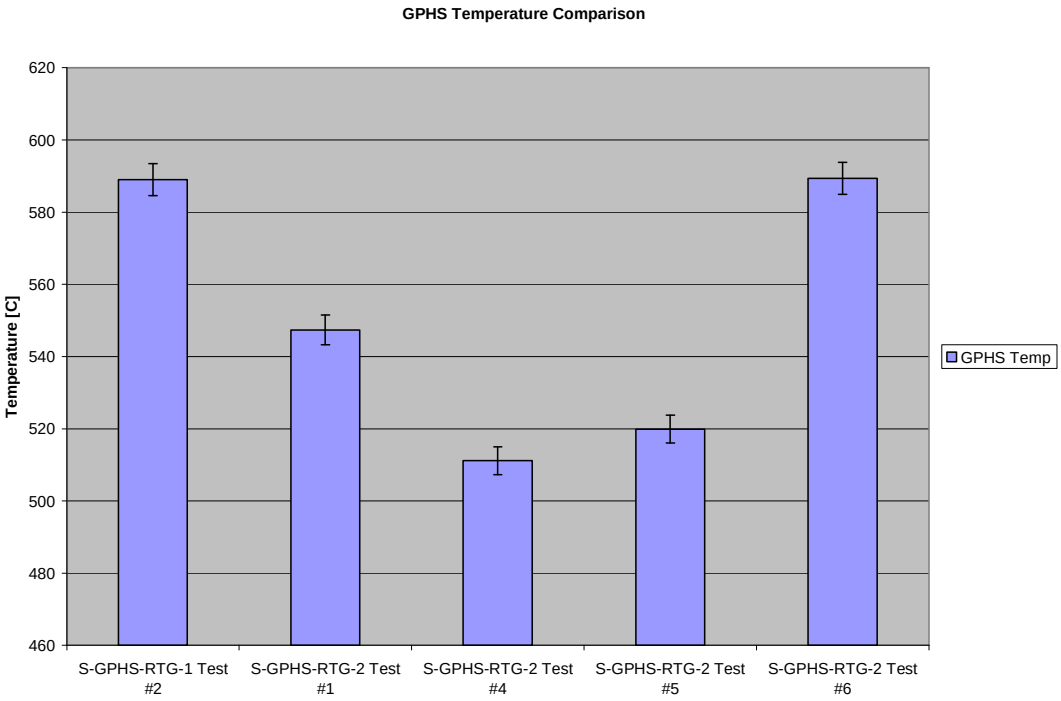

Figure 24. GPHS maximum temperature comparison

The above figure gives an interesting look at how various testing configurations affect the temperature of the GPHS. The second test of the S-GPHS-RTG-2 provided no GPHS temperature data because of a failed thermocouple. However, based on other measured values from that test, it is expected to be between 560˚C and 570˚C.

The composite insulation of Thermablok and Cabot aerogel insulation achieved higher internal temperatures than the entirely Cabot insulation package. This observation led to utilizing only Thermablok insulation in the final test, which yielded results nearing those of the S-GPHS-RTG-1.

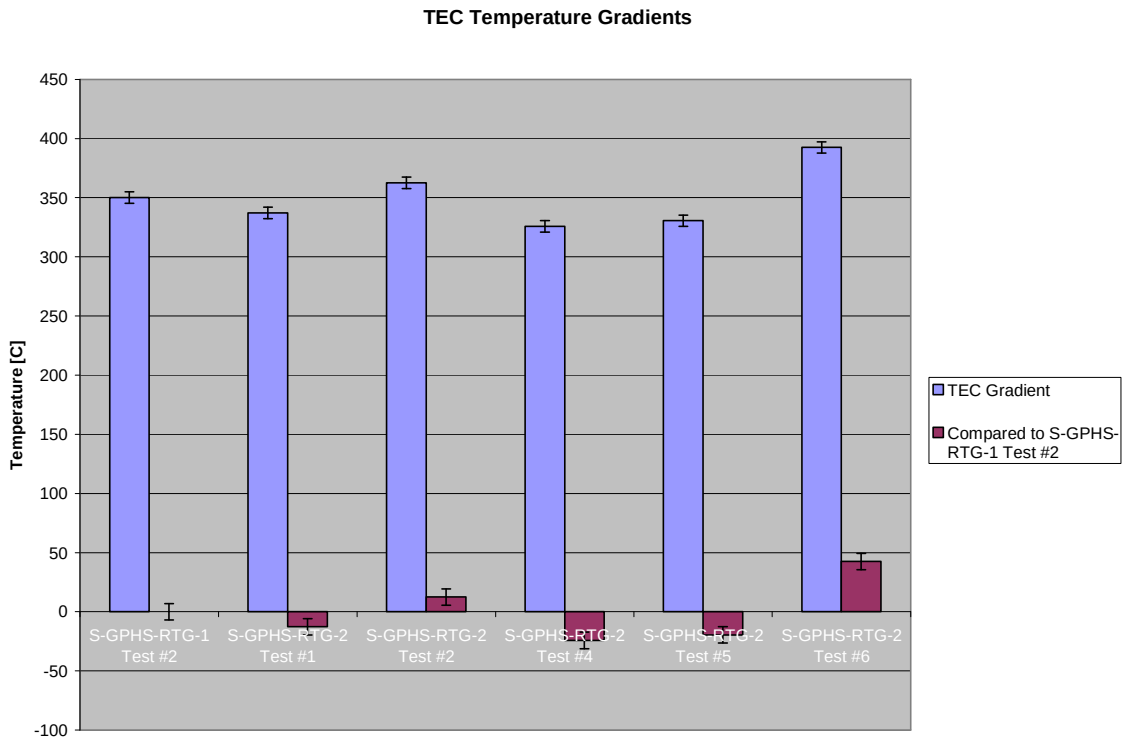

Figure 25. Comparison of TEC temperature gradients

The trend of the above graph shows that the composite aerogel insulation and entirely Thermablok insulation provide better TEC temperature gradients than the MLI and silica fiber composite used in the second S-GPHS-RTG-1 test. The purely Cabot aerogel insulation, however, was not able to achieve the same temperature gradient, though this may be closely related to the fact that the GPHS failed to reach comparable temperatures. The Cabot insulation acted as the primary insulation between the TEC's and the shell in the composite aerogel insulation, which did achieve some favorable results. Therefore, the Cabot aerogel's weakness can be observed in its inability to insulate the top and bottom of the GPHS. As the TEC temperature gradients drive the S-GPHS-RTG's ability to effectively produce electricity, maximizing this gradient is extremely important.

Compared to the aerogel's ability to insulate the GPHS, the TEC temperature gradients with the aerogel insulation are much higher than would be expected. This is clear evidence that the aerogel insulations provide better performance than the silica fiber insulation used in the second S-GPHS-RTG-1 test.

The behavior of the TEC temperature gradient with regard to MLI is unknown because only the first S-GPHS-RTG-1 test utilized MLI between the TEC's and the shell. By looking at the transient temperature data of the internal and external components of the second S-GPHS-RTG-1 test, it can be seen that internal and external components heat at different rates. Being as the first S-GPHS-RTG-1 test never reached steady state, its information regarding the comparison of internal and external components is void.

The bottom of the steady state S-GPHS-RTG-1 test surprisingly was cooler than the top. It would be expected that the bottom would be warmer, as the GPHS rested on the bottom, as opposed to the top being slightly elevated, the bottom has less surface area to radiate heat, and the same insulation was used for both the top and bottom. No simple answer exists for why the top plate of the S-GPHS-RTG-1 had a higher steady state temperature than the bottom. It is presumed to be caused by the asymmetry of the S-GPHS-RTG-1's design in isolating the top plate from the cooling fins. It could also be caused by the test itself, and as the sample size for steady state tests is so small, the numbers should perhaps be viewed cautiously.

In the S-GPHS-RTG-2 tests, the bottom plate was consistently warmer (~10˚C) than the top plate. This difference was very small (2˚C) in the final test which used Thermablok insulation throughout the device. The cause of this discrepancy is thought to be the weight of the GPHS bearing down and compressing the insulation on which it

rested. As aerogel's insulating properties are largely derived from the empty space within the substance, such pressure likely affected its ability to insulate the GPHS. The aerogel is also rather fragile and the insulation may have been effectively thinner below the GPHS. The smaller difference in the final test may have been due to the fact that some of the Thermablok insulation used had been used in previous tests and the top insulation may have already felt the compression's effects.

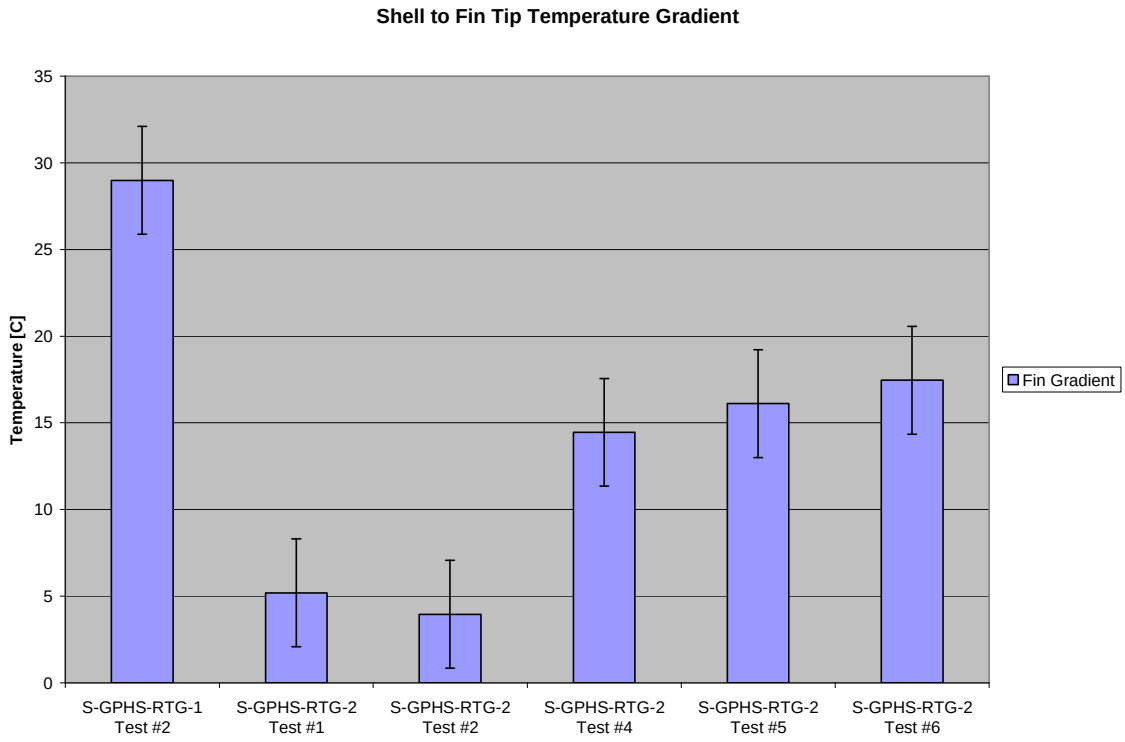

Figure 26. Comparison of fin temperature gradients

The higher temperature gradient across the fins seen in the S-GPHS-RTG-1 test compared to the S-GPHS-RTG-2 tests is expected because the S-GPHS-RTG-1 experienced higher temperatures at the shell. Because the cooling fins of the S-GPHS-RTG-1&2 are of comparable size the higher temperatures of the S-GPHS-RTG-1 fins caused more radiative heat loss and thus a larger temperature gradient.

7. CONCLUSIONS

The fact that the first two S-GPHS-RTG-2 tests had such low temperature gradients in comparison to later tests is more difficult to explain, as the fins in that test were comparable to those of any of the other tests. Another possibility lies in the fact that the fins of the S-GPHS-RTG-2 were not welded on in a totally uniform manner. The most even and similarly welded fins were chosen for data sampling. However, the first tests utilized a different fin than did later tests, and this uneven welding could be the cause of discrepancies.

The charred condition of the Thermablok blankets after the tests is also cause for major concern. While it may not be relevant, it more likely indicates outgassing and degraded performance. The fact that despite this the Thermablok blankets provided the tests with the highest internal temperatures is an impressive testament to their reliability. Heat cleaning the samples in a vacuum furnace to temperatures near what are expected to be seen in experiments may yield more favorable results. The Thermablok insulation is not intended for high temperatures, and utilizing similar insulation that is designed with the intent of surviving high temperatures may provide better results yet.

The Thermal Desktop models failure to provide accurate results is likely caused by inadequate material property data. Many assumptions had to be made about the materials used in the models, especially in regard to the insulation. Many of these materials had limited information available for conditions at room temperature and atmospheric conditions, much less the high temperature and vacuum regions in which they are expected to perform. Without accurate material property data, the solutions provided by the computer will be fundamentally flawed. In future studies, more time should be

devoted to the benchmarking of these virtual models against physical tests and obtaining reliable material properties. Sensitivity tests with the material property data could provide insight into how much inconsistencies affect the model.

A large concern for the S-GPHS-RTG is that the top and bottom of the GPHS lack any TEC's to collect heat. This is of major concern because they amount to more than one third of the GPHS's total surface area. If a uniform surface heat flux can be assumed, then over 80 W of heat is lost without any chance to be converted into electricity. The top and bottom of the GPHS are also in direct contact with insulating materials, while the sides only radiate heat to the TEC's. This likely caused even more heat to be wasted. Leaving the issue of heat loss through the top and bottom of the S-GPHS-RTG unaddressed will likely handicap the device's performance to the point of futility.

As of now, no solid ideas have been generated for how to suspend the GPHS within the device. In past RTG's this has been accomplished by something along the line of bolts coming in from the top and bottom. Previous RTG's had the luxury of multiple GPHS's to offset the heat lost through these bolts. This method of securing the GPHS is not expected to be a viable option for the S-GPHS-RTG, as it would likely increase the amount of unutilized heat lost through the top and bottom of the device. For the experiments performed in this study, the GPHS was allowed to simply rest on the bottom of the device. Some options were presented to suspend the GPHS, including the use of titanium wires to cradle it. However, none of these suggestions proved to be reasonably accomplishable for this study.

Ideally, the GPHS would be secured by some kind of TEC that would serve the double function of collecting heat and keeping the GPHS in place. Modular use of multiple S-

GPHS-RTG's would also decrease the total amount of heat lost. These heat loss issues must be addressed in order for the S-GPHS-RTG to be a viable power source for future missions.

8. BIBLIOGRAPHY

[1] Rinehart G. H. “Design Characteristics and Fabrication of Radioisotope Heat Sources for Space Missions.” Progress in Nuclear Energy. 39.3 (2001): 305-319. Print.

[2] Pantano, David R., and Dennis H. Hill. "Thermal Analysis of Step 2 GPHS for Next Generation Radioisotope Power Source Missions." *AIP Conference Proceedings* 746.1 (2005): 827-834. *Academic Search Premier*. EBSCO. Web. 5 May 2010.

[3] Wong, Wayne A., Anderson, David J., Tuttle, Karen L., Tew, Roy C. "NASA Radioisotope Power Conversion Technology NRA Overview." *AIP Conference Proceedings* 746.1 (2005): 421-428. *Academic Search Premier*. EBSCO. Web. 6 May 2010.

[4] Kasap, S. Thermoelectric Effects in Metals: Thermocouples. University of Saskatchewan, 2001. Web. 6 May 2010.

[5] United States. NASA. JPL. “Technologies of Broad Benefit- Power.” Mars Science Laboratory. NASA, Web. 6 May 2010.

[6] Woods, Brian G., Lindsay C. Arnold, and Tibor S. Balint. "Thermal Analysis and Testing of a Small Radioisotope Power System Concept." *AIP Conference Proceedings* 813.1 (2006): 348-355. *Academic Search Premier*. EBSCO. Web. 5 May 2010.

[7] Balint, Tibor S., and Emis, Nickolas D. "Validation Database Based Thermal Analysis of an Advanced RPS Concept." *AIP Conference Proceedings* 813.1 (2006): 327-333. *Academic Search Premier*. EBSCO. Web. 5 May 2010.

[8] Fricke, J., U. Heinemann, and H.P. Ebert. "Vacuum insulation panels—From research to market." *Vacuum* 82.7 (2008): 680-690. *Academic Search Premier*. EBSCO. Web. 5 May 2010.

[9] Schmidt, George R., and Michael G. Houts. "Radioisotope-based Nuclear Power Strategy for Exploration Systems Development." *AIP Conference Proceedings* 813.1 (2006): 334-339. *Academic Search Premier*. EBSCO. Web. 5 May 2010.

[10] “Thermocouple Home Page.” OMEGA Engineering Technical Reference. OMEGA Engineering, Web. 4 May 2010.

[11] Incropera, F. P., Dewitt, D. P., Bergman, T. L., Lavine, A. S. Fundamentals of Heat and Mass Transfer, Sixth Edition. John Wiley & Sons, 2007. Print.

[12] “GM-10.” Graphite Store: Product Data Sheet. Graphite Store, Web. 6 July 2009.

[13] "Thermablok High Temp Description." Thermablok High Temp Data Sheet. Thermablok, Inc., Web 6 July 2009.

[14] Holman, J. P. Experimental Methods for Engineers, Fourth Edition. New York: McGraw-Hill, 1984. Print.